IEEE Open Journal of
Power Electronics

Received 11 October 2023; accepted 5 November 2023. Date of publication 8 November 2023;
date of current version 22 November 2023. The review of this paper was arranged by Associate Editor Telles Brunelli Lazzarin.

Digital Object Identifier 10.1109/OJPEL.2023.3331180

A Review of DC-DC Resonant Converter Topologies and Control Techniques for Electric Vehicle Applications

GUVANTHI ABEYSINGHE MUDIYANSELAGE (Student Member, IEEE), NILOUFAR KESHMIRI (Student Member, IEEE), AND ALI EMADI (Fellow, IEEE)

McMaster Automotive Resource Centre (MARC), McMaster University, Hamilton, ON L8P 0A6, Canada

CORRESPONDING AUTHOR: GUVANTHI ABEYSINGHE MUDIYANSELAGE (e-mail: abeysing@mcmaster.ca)

ABSTRACT Resonant converters are attractive for DC-DC converter applications of electric vehicles (EVs) due to their wide range of soft switching and less output filter requirements compared to dual active bridge (DAB) converters. However, the design and control implementation of resonant converters is comparatively challenging due to the nonlinearities introduced with the resonant tank. LLC and CLLC resonant converters are popular among the resonant converter topologies, while new topologies are being derived based on the basic resonant converter topologies. This paper conducts a review on the basic resonant converter topologies, modes of operation of the resonant converter, modeling and control techniques, and special design considerations for resonant converter design. Existing topologies and control techniques of resonant converters enabling the derivation of new converter topologies and control methodologies, are investigated.

INDEX TERMS CLLC, extended describing functions, frequency modulation, LLC, optimal trajectory control, resonant converter, state plane analysis, topology morphing, wide voltage range operation.

I. INTRODUCTION

With the increasing concern over the impact of Carbon Dioxide (CO_2) emissions, the world is pushing towards electrified transportation. Many countries have set goals for electrified transportation and policies to provide government incentives to support the development of EVs [1]. Passenger EVs are expected to reach 500 million globally by 2040 [2]. Therefore, the EV industry is in rapid development and provides tremendous research opportunities.

Efficient and power dense powertrains in EVs are enabled via improved energy storage systems, power electronics converters and electric machines [3]. As a result, power electronics converters are being thoroughly researched and are rapidly advancing with the recent developments in wide band gap (WBG) semiconductor devices.

Throughout the EV, multiple DC-DC converter units are present, such as the on-board charger and auxiliary power unit (APU). The battery chargers can be classified into on-board chargers (OBCs) and off-board chargers [2]. OBCs are in two types as: single-stage and two-stage (power factor correction stage and isolated DC-DC converter stage). Further classification of OBC is provided in [1].

SAE J1772, the North American standard for electrical connectors for EVs, states levels of charging for different charging methods [4]. AC level 1 and 2 are for EV OBCs with power levels from 1.44 kW to 1.92 kW and 5 kW to 19.2 kW, respectively. DC level 1 and 2 (commonly called level 3) are for off-board chargers with maximum power levels up to 9 kW and 400 kW, respectively [5]. The J plug or SAE J1772 connector is adopted in North America for AC level 1 and 2 charging. The combined charging system (CCS) type 1 connector supports both AC and DC charging [6]. To support AC three phase charging, North American standard SAE J3068 for medium and heavy duty EV charging was proposed in 2018 [7]. This standard encompasses three phase AC voltages of 480 V (up to 133 kW power output at 160 A DC) and 600 V (up to 166 kW power output at 160 A DC).

For EV applications, the converters need to achieve high efficiency and high power density while minimizing cost. DAB

converters, also known as phase shifted full bridge (PSFB) converters and resonant converters are the commonly used DC-DC converters for bidirectional EV battery charger applications [8]. Phase shift (PS) (single/extended/dual/triple) control is applied to DAB converters while frequency modulation (FM) is the conventional control technique applied to resonant converters [9], [10], [11]. The appropriate topology must be selected based on the specific application ratings and requirements. Both DAB and resonant converters have zero voltage switching (ZVS) ability, which reduces the semiconductor switching losses, improving the efficiency. However, DAB tends to lose ZVS at partial load conditions [12]. A comparison among full bridge (FB)/ half bridge (HB) DAB and resonant converters is presented in [8] and the CLLC resonant converter has shown higher efficiency against DAB because of the wider soft switching region.

In terms of control complexity, PS control of DAB is easier. Resonant converters benefit from FM in the vicinity of the resonant frequency (f_r) for maximum efficiency. In terms of design complexity, the DAB converter design has only the inductor calculation, while the resonant converter design has the resonant tank calculation, which consists of one or more capacitors and inductors in series/parallel/series-parallel configuration.

Since the resonant converter has nearly sinusoidal waveforms, their higher-order harmonic ripple content is less than that of DAB converters. Hence, the output filter requirement for DAB converters is more than that of resonant converters. The resonant converters can yield higher efficiency, but due to their design and control complexity, careful design consideration is required for a high power density converter with optimum control. Hence, this work is based on the design and control of resonant converters for DC-DC converter applications in EVs.

Resonant converters have been evolving since the 1940s with vacuum-tube power converters. They can achieve fast switching, low losses with soft switching, wide ranges of operating voltage, galvanic isolation, and high power density. With the rapid development in semiconductors, high frequency, power dense, and efficient resonant converters are highly suitable for DC-DC converters in EV applications.

There are four basic topologies of resonant converters: series, parallel, series-parallel, and LLC resonant converters. FB, HB, and center tapped configurations of primary and secondary bridges with Metal Oxide Semiconductor Field Effect Transistors (MOSFETs) and/or diodes are used with these topologies. Application specific new topologies are also derived based on these topologies. Resonant converters are modeled in both frequency and time domains, with different levels of accuracy in different regions of operation. The designer should be mindful to select the modeling approach based on the purpose and outcome of the model. While FM is the popular and conventional control technique for resonant converters, hybrid control techniques with PS and pulse width modulation (PWM) have also been implemented.

A review on resonant converter classifications is provided in [13] in terms of basic topologies and control schemes to provide a guideline to select a topology for EV applications. There, the discussion on control schemes is limited, while the authors focus more on comparison at the topology level, diving into unidirectional and bidirectional battery chargers. However, modeling techniques and design considerations specific to resonant converters are not discussed. Due to their complexity, the review of resonant converters at topology and control levels is insufficient for an optimized and efficient converter design.

A comprehensive analysis on DC-DC resonant converters with comparison among topologies, modeling, and control techniques is not sufficiently discussed in the literature. This paper aims to build on the basic topologies, resonant converter specific modeling and control techniques, and design considerations for EV applications. Due to the broad range of resonant topologies, the discussion is limited to voltage source DC-DC resonant converters. The authors expect this to be a foundation for the researchers to derive new resonant converter topologies and improve converter modeling, control and optimization techniques for evolving applications in the EV industry.

The rest of the paper is organized as follows. Section II conducts a review of DC-DC resonant converter topologies. Both conventional and novel topologies are investigated. Section III reviews resonant converter specific control techniques. Modeling techniques are presented in Section IV. Resonant converter design considerations, such as application overview, design optimization, component selection, transformer design, parasitic, and dead time analysis are briefed in Section V. Section VI discusses potential research directions and future prospects.

II. RESONANT CONVERTER TOPOLOGIES

One of the main selection criteria for DC-DC converters is the semiconductor losses. Semiconductor losses are categorized into conduction and switching losses. Turn-on switching losses occur when there is a voltage across the switch during turn-on and turn-off losses occur when there is non-zero current through the switch during turn-off. ZVS is switching at zero voltage across the switch. Zero current switching (ZCS) is switching at zero current through the switch.

Converters with a resonant tank (inductors and capacitors), enabling ZVS and/or ZCS, can be characterized as resonant converters [14]. Due to the broad range of resonant converters, different bases for classification, such as the number of resonant tank elements, resonant tank configuration, and modes of resonance, are offered in the literature [13], [14], [15]. Classification of DC-DC resonant converters based on the mode of resonance is provided in Fig. 1.

In load resonant converters, the resonant tank impedance is used to control the power flow to the load. The resonant tank impedance can be varied either through switching frequency (f_s) variation or other control techniques. These converters

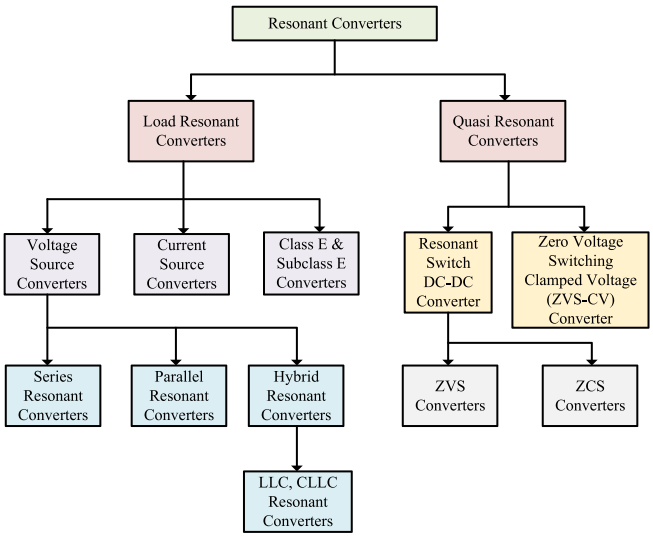

FIGURE 1. Resonant converter classification.

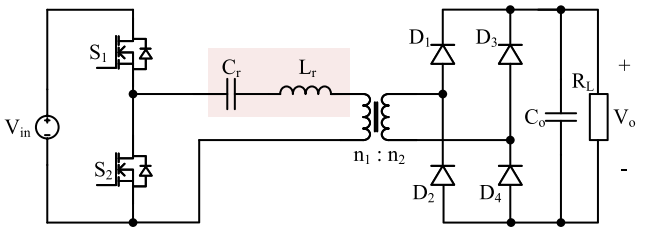

FIGURE 2. Half bridge series resonant converter.

can be further classified into voltage source, current source, and class E and subclass E resonant converters.

In quasi-resonant converters (or resonant switch converters) the resonant tank is used to manage the shape of the voltage and current waveforms to achieve ZVS and/or ZCS. In these converters, during one switching period, there are both resonant and non-resonant operating intervals. Furthermore, the DC-DC resonant converters can also be classified as isolated or non-isolated converters based on galvanic isolation between the two bridges. The focus of this paper will be on DC-DC isolated voltage source resonant converters, which are popular in EV applications.

A. SERIES RESONANT CONVERTER

The conventional HB series resonant converter (SRC), also known as DAB series resonant converter is shown in Fig. 2. A detailed analysis of the HB SRC with a normalized mathematical model is given in [16]. The impedance of the series resonant tank is varied using FM to regulate the voltage at the load, as in a voltage divider [13]. Hence, the DC gain of the SRC will always be less than unity (step down operation only).

SRC has a larger magnetizing inductance compared to the LLC resonant converter, resulting in smaller circulating currents, which leads to a higher efficiency at f_r. If $f_s >> f_r$, the resonant tank impedance limits the current through the converter, making it a short circuit proof converter [17].

Using the first harmonic approximation (FHA) analysis, the AC equivalent circuit of the resonant converters can be analyzed and the AC load equivalent to the DC load (R_L) in secondary side referred to the primary side, can be given as in (1) [18]. This derivation of R_e is valid to all the topologies discussed in this study.

$$R_{eq,ac} = \frac{8}{\pi^2}\frac{n_2}{n_1}R_L \tag{1}$$

The voltage gain (G) of the converter can be derived as a function of the normalized frequency ($\omega_n = \frac{\omega}{\omega_r}$) and Q-factor. Q-factor is the ratio between the characteristic impedance (Z_0) and $R_{eq,ac}$. This derivation is summarized from (2) to (4) where ω is the angular switching frequency and ω_r is the angular resonant frequency. The gain function in (4) can be plotted as a function of normalized frequency for varying Q-factors to select the best Q-factor for the resonant tank parameter calculations.

$$\omega_r = \frac{1}{\sqrt{L_r C_r}} \tag{2}$$

$$Q = \frac{Z_0}{R_{eq,ac}} = \frac{\omega_r L_r}{R_{eq,ac}} \tag{3}$$

$$G = \frac{\frac{n_1}{n_2}V_o}{V_{in}/2} = \frac{1}{\sqrt{1 + Q^2(\omega_n - \frac{1}{\omega_n})^2}} \tag{4}$$

PWM control techniques at fixed f_s have been widely studied to improve the operating voltage range with both step-up and step-down functionality while improving the efficiency of the SRC [19], [20]. However, ZVS could be lost in certain regions of operation. In [20], PWM control and topology morphing has been applied to the SRC for a universal EV charger application with buck-boost operation. The SRC topology proposed in [21] is a bidirectional FB SRC with PWM control, which can operate under a wide output voltage range by using a voltage doubler on the secondary. It operates as a conventional FB SRC in the forward power flow direction and as a HB resonant boost converter in the reverse direction.

A main disadvantage of the SRC is its inability to control the DC output voltage at no load or light load [13], [17]. According to [17] and as seen from (3) and (4), the SRC will operate under a very high f_s to control the output voltage at light loads. Several techniques have been proposed to rectify this issue, which includes topological and control changes [17], [22], [23]. A hybrid control technique with frequency and duty cycle control is proposed in [23] with a promising 4% increase in efficiency at light load compared to FM.

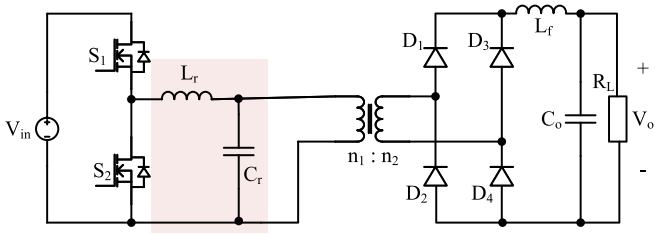

FIGURE 3. Half bridge parallel resonant converter.

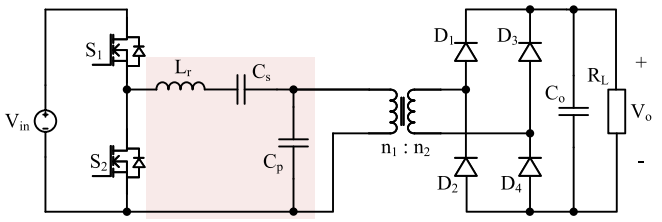

FIGURE 4. Half bridge series-parallel resonant converter.

B. PARALLEL RESONANT CONVERTER

A HB parallel resonant converter (PRC) topology is given in Fig. 3. An inductor (L_f) is added in the secondary output to match the impedance [24]. Similar to SRC, the voltage gain for PRC can be derived as in (5) and (6).

$$Q = \frac{R_{eq,ac}}{\omega_r L_r} \tag{5}$$

$$G = \frac{\frac{n_1}{n_2}V_o}{V_{in}/2} = \frac{1}{\sqrt{(1-\omega_n^2)^2 + (\frac{\omega_n}{Q})^2}} \tag{6}$$

In contrast to SRC extracting energy from the circulating resonant current, in PRC, energy is transferred from the parallel connected resonant inductor or capacitor [25]. The main advantage of PRC over SRC is the no load operation [26]. Hence, PRC is preferred for applications with wide range of load variations over SRC [27], [25]. Similar to SRC, PRC is also naturally short circuit proof. Load insensitivity of PRC is an advantage [26]. However, load independent circulating currents, which could lead to high conduction losses could also be a major disadvantage of the PRC [28].

Both SRC and PRC can operate either in continuous conduction mode (CCM) or discontinuous conduction mode (DCM). In CCM, the current through the resonant tank never reaches zero during a switching period (T_s). When the switch is turned on, current through the anti-parallel diode will rapidly transfer to the switch [29]. In DCM, the current through the resonant tank terminates, facilitating ZVS in the primary bridge and ZCS in the secondary bridge [30]. However, DCM also has the disadvantage of high current and voltage peaks [31].

Apart from FM, a few other control techniques have been studied for PRC in [27], [32], [33] and [34]. In [27], a robust controller designed from μ-synthesis is presented [35]. A control method called resonant tank control (RTC) is proposed in [34] for operation above f_r. There, a linear combination of resonant capacitor voltage and resonant inductor current is used to define the control law.

C. SERIES-PARALLEL RESONANT CONVERTER

Series-parallel resonant converter (SPRC), (or LCC converter) has the combined advantages of both SRC and PRC, while eliminating their drawbacks, such as lack of no load regulation in SRC and circulating currents in PRC [36], [28]. The conventional HB SPRC topology is given in Fig. 4. Here, ω_r is defined with respect to C_r as given in (7). The series Q-factor (Q_s) for SPRC can be defined as in (8) and the parallel Q-factor (Q_p) will be the reciprocal of Q_s.

$$\omega_r = \frac{1}{\sqrt{L_r C_{rs}}} \tag{7}$$

$$Q_s = \frac{\omega_r L_r}{R_{eq,ac}} \tag{8}$$

Hence, the voltage gain for SPRC is derived as given in (9).

$$\frac{\frac{n_1}{n_2}V_o}{V_{in}/2} = \frac{1}{\sqrt{\left[1+\frac{C_p}{C_s}(1-\omega_n^2)\right]^2 + \left[Q_s(\omega_n - \frac{1}{\omega_n})\right]^2}} \tag{9}$$

At full load, the effective load resistance will be low enough to approximately bypass C_p and the SPRC will behave as an SRC. At light or no load, C_p will be effective and the ω_r of the circuit will be updated with the equivalent capacitance of two resonant capacitors as given in (10) [28]. This can be visualized from the plot of voltage gain obtained from (9). The Q-factor will also change from Q_s to Q_p when moving from full-load to light load, changing the converter characteristics from SRC to PRC.

The value of C_p should be large enough to provide sufficient no load regulation but small enough to reduce the load independent circulating currents. In [28], $C_p = C_s$ is considered as an acceptable design compromise.

$$\omega_r = \frac{1}{\sqrt{\frac{L_r C_s C_p}{C_p + C_s}}} \tag{10}$$

SPRC can also operate in both CCM and DCM with either FM or PS control at fixed f_s [29], [37]. Optimum trajectory control (OTC) is another control technique studied for SRC, PRC and SPRC to manage transients between steady states of nonlinear resonant converters. In SPA, SPRC has 3 states in the resonant tank compared to 2 states in SRC and PRC. In [38], a generalized OTC method for transitions between any 2 states of SPRC is proposed. OTC will be discussed further in Section III.

D. LLC AND CLLC RESONANT CONVERTER

A FB LLC converter is shown in Fig. 5, which is preferable over HB converters in EV battery charger applications due

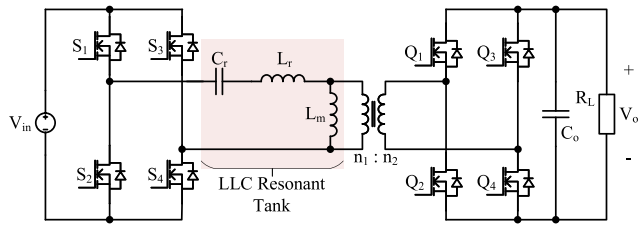

FIGURE 5. Full bridge LLC resonant converter.

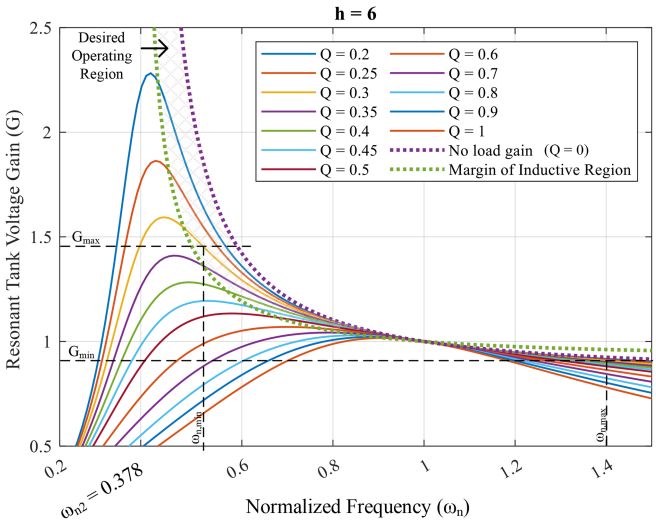

FIGURE 6. Plot of LLC Converter Voltage Gain vs Normalized frequency for different Q factors at $h = 6$.

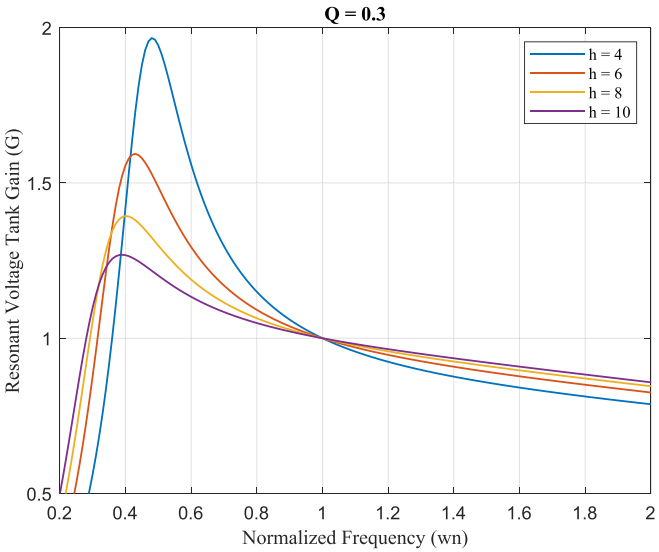

FIGURE 7. Plot of LLC Converter Voltage Gain vs Normalized frequency for different h ratio at $Q = 0.3$.

to their high power ratings [18]. In Fig. 5, the secondary bridge is a FB of MOSFETs instead of diodes to minimize the conduction losses and implement synchronous rectification (SR), which will be discussed in Section III. The primary ω_r is derived based on the series resonant tank, as shown in (11).

$$\omega_r = \frac{1}{\sqrt{L_r C_r}} \tag{11}$$

The voltage gain formula for the LLC converter can be derived using FHA of the equivalent AC circuit as in (12) and (13) where $h = \frac{L_m}{L_r}$. The Q-factor for the series resonant tank is defined below.

$$Q = \frac{\omega_r L_r}{R_{eq,ac}} \tag{12}$$

$$G = \frac{\frac{n_1}{n_2} V_o}{V_{in}} = \frac{1}{\sqrt{(1 + \frac{1}{h} - \frac{1}{h\omega_n^2})^2 + Q^2(\omega_n - \frac{1}{\omega_n})^2}} \tag{13}$$

In Fig. 6, a group of plots for different Q-factors for the voltage gain function given in (13) is shown. This plot can be compared against the voltage gain plots of SRC, PRC, and SPRC, as presented in [28]. The desired operation is at the vicinity of ω_r, as it is independent of the load at $f_s = f_r$.

Additionally, voltage gain is also dependent on the inductance ratio h, as observed in Fig. 7. Comparison between the characteristics of LLC and SPRC converters shows that both converters have no load controllability and wide voltage range capability with boost operation. However, both topologies have the cost of circulating currents. But, SPRC needs an additional parallel capacitor. In LLC converters, the circulating currents will decrease with the load. In SPRC converters, the circulating currents will not decrease with the load after it fully assumes the PRC characteristic [28]. A second resonant frequency (ω_{r2}) for no load operation is defined in (14). The gain characteristic in Fig. 6 is divided into capacitive (left) and inductive (right) regions. The margin between the regions is determined based on the resonant tank input impedance, provided in (15) [18]. It is desired to operate in inductive region with $\omega_s > \omega_{r2}$ to inherit ZVS.

$$\omega_{r2} = \frac{1}{\sqrt{(L_r + L_m)C_r}} = \omega_r \sqrt{\frac{1}{1+h}} \tag{14}$$

$$G_{critical} = \frac{h\omega_n}{\sqrt{h[\omega_n^2(h+1) - 1]}} \tag{15}$$

At higher h, the peak voltage gain decreases and the range of f_s widens, resulting in high switching losses and vice versa for lower h at the cost of higher circulating currents. Therefore, the selection of h is a compromise between a wide range of f_s and high magnetizing currents. The rule of thumb is to maintain $h > 4$ to minimize the losses due to magnetizing current.

If LLC converter is used for bidirectional operation, the converter will operate as an SRC in the reverse direction. Hence, the CLLC (or CLLLC) converter, demonstrated in Fig. 8 is the bidirectional topology of LLC converter, with an additional series resonant tank on the secondary side. The voltage gain for the CLLC converter for two directions of power flow can be derived similar to LLC. The voltage gain

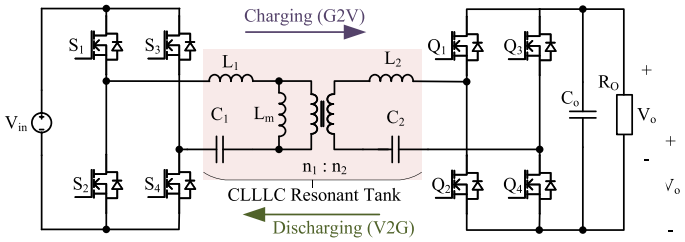

FIGURE 8. Full bridge CLLC resonant converter.

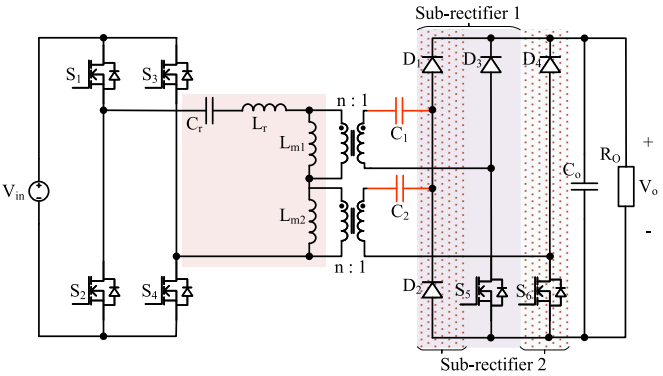

FIGURE 9. LLC with reconfigurable hybrid voltage multiplier [39].

for charging mode (G2V) is given in (16) where $k = \frac{n_1^2}{n_2^2} L_2/L_1$ and $g = \frac{n_1^2}{n_2^2} C_2/C_1$ [8].

$$G = \frac{\frac{n_1}{n_2} V_o}{V_{in}} = \frac{1}{\sqrt{a^2 + b^2}} \tag{16}$$

$$a = \frac{1}{h} + 1 - \frac{1}{h\omega_n^2} \tag{17}$$

$$b = \left(\frac{k}{h} + 1 + \frac{1}{gh} + \frac{1}{g}\right)\frac{Q}{\omega_n} - \left(\frac{k}{h} + 1 + k\right) Q\omega_n - \frac{Q}{gh\omega_n^3} \tag{18}$$

E. RECONFIGURABLE RESONANT CONVERTERS

A main drawback of topologies discussed above is the wide range of f_s for wide voltage range applications. This leads to challenges in optimizing the converter magnetics, high circulation currents, and switching losses. To address these, new reconfigurable topologies have been derived.

1) LLC CONVERTER WITH RECONFIGURABLE RECTIFIER

An LLC converter with a reconfigurable rectifier proposed in [39] for wide output voltage range applications is presented in Fig. 9. This topology has 2 sub-rectifiers (sub-R) in parallel, which can be extended to add extra sub-rectifiers for ultra-wide voltage range applications. This rectifier can operate under 3 modes: 1) FB rectifier mode for low output voltage, where both sub-Rs operate with SR; 2) hybrid voltage multiplier rectifier mode for nominal output voltage, where S_6 is always on, such that sub-R 1 acts as a FB rectifier and sub-R 2 acts as a voltage doubler; 3) voltage multiplier rectifier mode for high output voltage, where both S_5 and S_6 are on, such that both sub-Rs act as voltage doublers. This uses FM, while PS control is used for smooth transition among the rectifier modes. However, this topology requires two transformers or a multi-winding transformer compared to regular LLC converters.

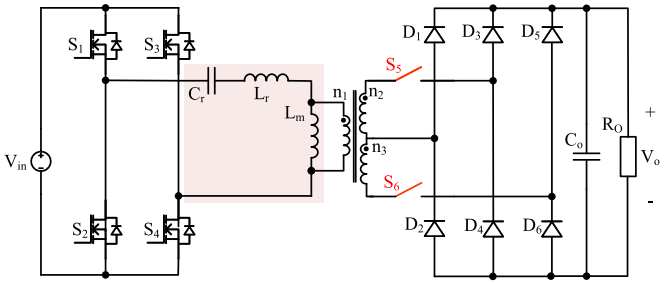

FIGURE 10. LLC with Adjustable *n* and Reconfigurable Rectifier [40].

2) LLC CONVERTER WITH ADJUSTABLE TURNS RATIO AND RECONFIGURABLE RECTIFIER

A topology with the same design objective discussed above, is proposed in [40] and given in Fig. 10. This topology has an adjustable turns ratio, where the secondary winding of the transformer has an extra tap, so the secondary turns can vary among three combinations: n_2, n_3, and $n_2 + n_3$. It has bidirectional switches S_5 and S_6 with four-quadrant operation for turns selection. The primary bridge uses topology morphing to change between FB and HB. There are four modes of operation: 1) primary bridge as a HB with S_5 on; 2) primary bridge as a FB with S_5 on; 3) primary bridge as a FB with S_6 on; 4) primary bridge as a FB with both S_5 and S_6 on. With the 4 modes of operation, the range of voltage gain is reduced by four folds while maintaining f_s close to f_r. The authors have obtained 90%–97.5% efficiency for a 60 V–450 V output voltage experimental setup.

F. HYBRID RESONANT CONVERTERS

New resonant converter topologies are derived in hybrid with other topologies, which use FM, PS control or PS-FM hybrid control. Converters with PS control offer the advantages of both PSFB and resonant topologies while compensating each other's drawbacks. They overcome the disadvantages of PSFB converters, such as narrow ZVS range and absence of ZCS and the disadvantages of resonant converters, such as wide range of f_s for wide voltage range operation [41], [42].

1) CAPACITOR-CLAMPED LLC CONVERTER

While PS control can be implemented in conventional resonant converters, new topologies have also been introduced with PS control, mainly for wide voltage range applications

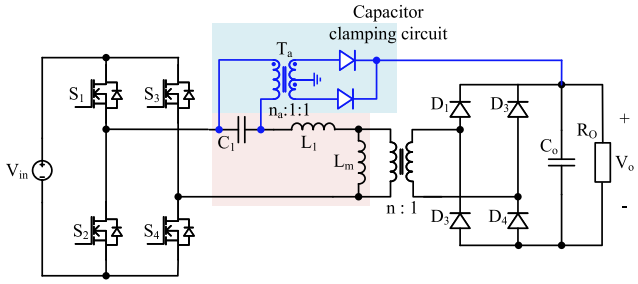

FIGURE 11. Capacitor-clamped FB LLC converter [42].

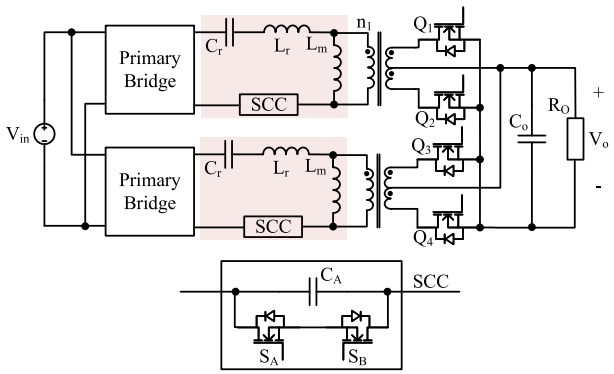

FIGURE 12. Interleaved Multi-Phase LLC Converter.

of OBCs. A fixed f_s, phase shifted capacitor-clamped FB LLC converter is proposed in [42], which claims to achieve a wider ZVS range and smaller PS range compared to phase shifted LLC converters. Hence, it is a promising topology for wide voltage range applications. The proposed topology is given in Fig. 11, with a capacitor voltage clamping circuit in addition to the conventional LLC topology. It clamps the voltage of C_1 (v_{C1}) to nVo. Limiting v_{C1} aids in discharging the energy stored in L_m faster to ensure ZVS.

2) LLC/CLLC -NPC HYBRID CONVERTERS

The LLC or CLLC converters in hybrid with 3-level (3 L) neutral point clamped (NPC) converter and 5-level (5 L) NPC converter are proposed in the literature for reducing the voltage stress of the switches in high voltage (HV) EV applications, such as off-board battery chargers [43], [44], [45]. The CLLC-NPC hybrid converter is proposed in [44]. This is a FB CLLC topology, as shown in Fig. 8, where each leg is replaced with a 3L-NPC arm. The 3-levels of voltage in each NPC arm will form 4 modes for each FB such that the bridge voltage can vary within $[-V_{in}, V_{in}]$, $[-0.5V_{in}, V_{in}]$, $[-0.5V_{in}, 0.5V_{in}]$ and $[0, 0.5V_{in}]$. Altogether, this will form 16 modes under FM and the process of selecting the optimal model is described in [44].

G. INTERLEAVED RESONANT CONVERTERS

Interleaved LLC converters are proposed for both on-board and off-board battery chargers, and on-board low voltage DC-DC converters (interfaces HV battery with low voltage APU) [46], [47]. Parallel inputs will facilitate load shedding at light load [46]. Also, in cases where it is not possible to realize a small L_m required by the high current design, multi-phase interleaved LLC design is considered [48]. An interleaved multi-phase (parallel input) LLC is given in Fig. 12 for high current applications. The primary bridge can be a regular HB, FB or a FB with two 3 L NPC arms [49]. For applications with high output voltage, the secondary bridge can also be replaced with a cascaded voltage doubler [47].

Ensuring balanced current sharing in interleaved multi-phase LLC converters is a challenge. At $f_s \approx f_r$, the impedance of the resonant tank is too small that even a small change in resonant tank values may result a significant change in impedance causing current imbalance. Hence switch controlled capacitor (SCC) method is used [50]. An additional resonant capacitance C_A is controlled using the bidirectional switches S_A and S_B to control the total resonant capacitance: $C_1//C_A$. The control of these bidirectional switches is based on zero crossing of the resonant tank current and voltage of C_A [46].

This topology can use either the PS control or FM [50], [51]. In PS control, the PS between phases is controlled for output current ripple cancellation [50]. In FM, all phases operate at the same f_s, with all the gate signals interleaved to facilitate ripple cancellation in the output current [51].

A comparison among the topologies discussed in this Section is given in Table 1. When selecting the topology, the voltage and power levels of the application, power density and volume constraints, design complexity, reliability, and cost should be considered. For OBC applications, the volume is constricted; hence, high power density is desired. Therefore, LLC or CLLC converters with a lesser number of components compared to new topologies discussed above are suitable. For off-board chargers, the HV, high power converters, such as hybrid and reconfigurable topologies discussed above are preferred, where volume is not restricted like in OBCs. The control technique can be selected based on the voltage range of operation to maximize the peak or overall efficiency based on battery charging profiles.

III. RESONANT CONVERTER CONTROL TECHNIQUES

Resonant converter control techniques can be classified into FM and PWM techniques. This Section will discuss these control techniques with reference to LLC and CLLC resonant converters.

A. CLASSICAL FREQUENCY CONTROL TECHNIQUE

FM is the classical control technique related to resonant converters, allowing them to operate in both CCM and DCM. FM gives the ability to reach high frequencies and soft switching capability. In frequency control, the switches in each leg of the primary bridge are operated complementary to each other with 50% duty ratio. Therefore, dead time (also known as

TABLE 1. Comparison Among Conventional and New Resonant Converter Topologies

Topology	SRC [21]	SPRC [52]	LLC [53]	CLLC [54]	LLC + recon. rectifier [39]	LLC with adj. n [40]	Cap. clamped LLC [42]	CLLC + NPC Hybrid [44]
Resonant Capacitors	1	2	1	2	1	1	1	1
Resonant Inductors	1	1	1	2	1	1	1	1
Limit L_m?	no	no	yes	yes	yes	yes	yes	yes
Topology arrangement	FB at primary, volt. doubler at secondary	FB at primary, curr. doubler at secondary	FB at primary and secondary					
FET count	6	6	4	8	6	8	4	16
Diode count	0	0	4	0	4	6	6	8
Capacitors	2	0	0	0	2	0	0	8
Gain range	0 - 1		0.975 - 1.9	G2V: 0.7 - 1.2 V2G: 0.8 - 1.5	V_2[] reduce by x1.5	0.15 - 1.15	0.587 - 0.987	wide V_2 = 200 - 700V
Control	PS	PS + FM	FM	FM	FM	PS	PS	FM
Peak efficiency	97.80%	95.30%	97.96%	G2V - 97.9% V2G - 98.06%	97.60%	97.50%	98.03%	G2V - 96.5% V2G - 96.8%
Power rating	3.3 kW	500 W	6.6 kW	1 kW	3.3 kW	1.8 kW	825 W	3.5 kW
Soft switching	ZVS, ZCS (except bottom 2 FETs of primary FB)	ZVS for partial range, ZCS from SR	ZVS and ZCS ($f_s < f_r$)	ZVS and ZCS ($f_s < f_r$)	ZVS	ZVS and ZCS for partial range	ZVS and ZCS	
Special features	Less circulating currents	improved light load regulation	Lm is a part of the res. tank	bidirectional power flow	preferred for wide input/voltage range applications			for wide voltage range and high power app.

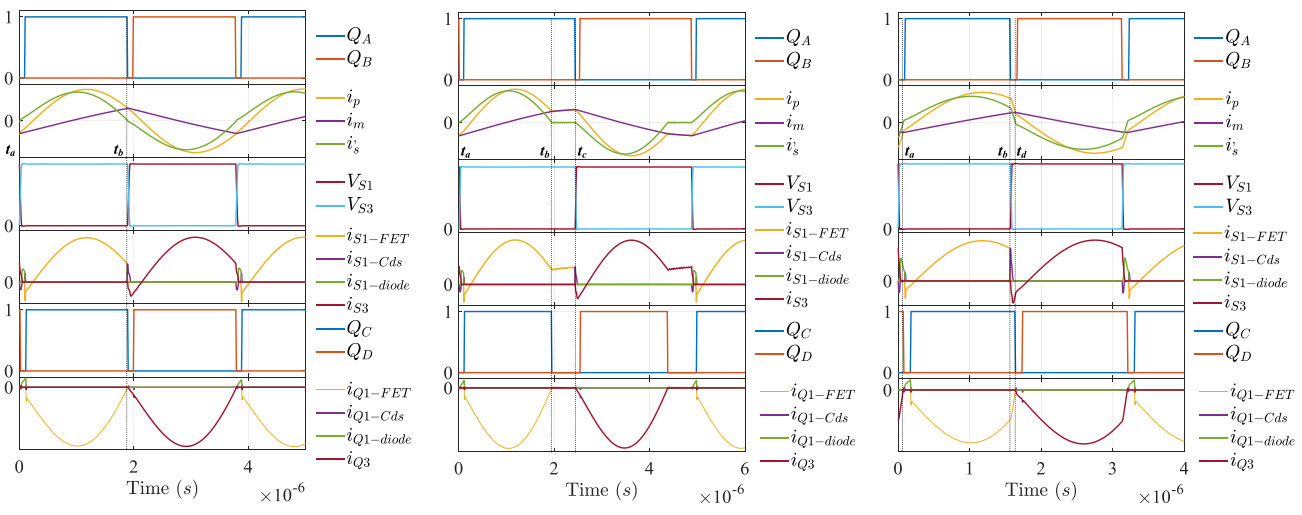

(a) $f_s = f_r$ (b) $f_s < f_r$ (c) $f_s > f_r$

FIGURE 13. LLC converter waveforms.

dead band time) is introduced between the switches in each leg to permit transitions, preventing a short circuit [55]. The secondary bridge MOSFETs will turn-on at the same time as primary bridge MSOFETs and turn-off based on SR.

The operation with FM should be studied for $f_s = f_r$, $f_s < f_r$ and $f_s > f_r$ to understand the CCM and DCM operation. Fig. 13 provides the LLC converter simulated waveforms for operation under these 3 cases. Current

through the MOSFET during the conduction period (i_{S1-FET}, i_{Q1-FET}), current through the MOSFET output capacitance (i_{S1-Cds}, i_{Q1-Cds}) and current through the MOSFET body diode ($i_{S1-diode}$, $i_{Q1-diode}$) are illustrated separately for MOSFET S_1 of the primary bridge and MOSFET Q_1 of the secondary bridge to understand different conduction paths in the converter and soft switching during a single switching period. Conduction paths of the CLLC converter is given in [56].

1) SYNCHRONOUS RECTIFICATION AT THE SECONDARY BRIDGE

In the LLC converter given in Fig. 5, the secondary bridge has MOSFETs instead of diodes to minimize the conduction losses, as the internal resistance of MOSFETs is lower than that of diodes. The gate signals for the secondary bridge are similar to those of the primary bridge. However, to minimize the switching losses in the secondary bridge, SR can be used [57], [58], [59]. In SR, the MOSFETs are turned off when the current through the MOSFETs reaches zero (i.e., at the zero crossing of the secondary AC current i_s).

Several techniques for SR implementation are discussed in the literature. In [57], SR is implemented by analyzing the PS between primary and secondary AC currents. To minimize the effects of circuit parasitics, SR gate signals can be generated by voltage or current sensing. A comparison among approximation based and measurement based SR techniques proposed in the literature for LLC converters is provided in [59]. This analysis shows that approximation based SR techniques are easy to implement, but they do not have sufficient accuracy through out the whole range of f_s. Also, approximation based techniques can be applied to a constrained range of frequencies. Current based SR techniques can be applied to applications with a wide range of f_s, both below and above resonance operation, at the cost of decreasing power density due to AC current sensing. It is also noted that primary current based SR techniques have high reliability, improved power density, and efficiency compared to secondary current based SR techniques, but at the cost of control complexity to decouple the magnetizing current [59].

2) OPERATION AT RESONANT FREQUENCY ($f_s = f_r$)

Fig. 13(a) gives current and voltage waveforms with gate signals for operation at f_r. SA is the gate signal for S_1 and S_4, SB is the gate signal for S_2 and S_3. Similarly, QA for Q_1 and Q_4, QB for Q_2 and Q_3. During the dead time $(0 - t_1)$ after switches S_3 and S_2 turn-off, the output capacitance of S_1 and S_4 are discharged and the output capacitance of S_3 and S_2 are charged. Then, the anti-parallel body diodes of S_1 and S_4 conduct, forcing the voltage across the respective switches to zero. Hence, S_1 and S_4 will achieve ZVS at turn-on. The primary current (i_p) meets the magnetizing current (i_m) at turn-off. Hence, the primary bridge MOSFETs will turn-off at very low turn-off currents (low turn-off losses).

In the secondary bridge, the MOSFETs will have ZVS at turn-on due to the capacitor and diode conduction during the dead time, similar to the primary bridge. They will turn-off with ZCS as the secondary current (i_s) reaches zero when $i_p = i_m$. Also, the secondary gate signals are equivalent to the primary gate signals and SR has not been applied as the gate signals turn-off exactly when i_p reaches i_m.

3) BELOW RESONANCE OPERATION ($f_s < f_r$)

Fig. 13(b) demonstrates the current and voltage waveforms with gate signals for operation below f_r. Both primary and secondary bridges have ZVS at turn-on, due to diode conduction during the dead time $0 - t_1$. Secondary bridge MOSFETs Q_1 and Q_4 turn off with SR at the zero crossing of i_s. They achieve ZCS at turn-off. During the time interval $t_2 - t_3$, there is a circulating current with $i_p = i_m$, and zero power flow in the primary bridge until the primary bridge MOSFETs S_1 and S_4 turn-off. This can be identified as DCM operation.

4) ABOVE RESONANCE OPERATION ($f_s > f_r$)

Fig. 13(c) shows the current and voltage waveforms with gate signals for operation above f_r. Both primary and secondary bridges inherit ZVS at turn-on. S_1 and S_4 turn-off before Q_1 and Q_4. Hence, there will be no circulating currents on the primary bridge. Therefore, this can be identified as CCM operation. However, as the primary bridge MOSFETs turn-off before i_p reaches i_m, there will be higher turn-off switching losses compared to the previous two cases. Secondary bridge MOSFETs turn-off with ZCS due to SR.

A comparison among the three modes of operation is given in Table 2.

The operation of the CLLC converter will be similar to the above analysis. The LLC and CLLC converters can operate in both DCM and CCM modes under FM, achieving ZVS and ZCS. In order to realize ZVS, the magnetizing current should be sufficiently large to charge and discharge the MOSFET output capacitance ($C_{DS} = C_{oss} - C_{rss}$) completely during the dead time (t_d) [8], [60]. A condition derived for the dead time to satisfy this for a FB converter is given in (19) [61].

$$L_m \leq \frac{t_d}{8 C_{DS} f_{s,\max}} \tag{19}$$

Based on the expected range of voltage gain: $G_{\max}$ to $G_{\min}$ in Fig. 6, the normalized operating frequency range can be identified as $\omega_{n,\min}$ to $\omega_{n,\max}$. It should be noted that the accuracy of the gain plot approximated based on FHA, decreases when moving away from f_r [56].

The CLLC converter operation requires to identify the direction of power flow. A decision algorithm based on dead time control is proposed in [56]. The LLC and CLLC topologies discussed here can also be extended to three-level converters with the same resonant tank to operate in wide ranges of voltage with narrow frequency range [62], [63].

Based on the small signal model analysis discussed in Section IV, a linear compensator (PI or PID controller) or a nonlinear compensator (lead or lag compensator) can be designed for the closed loop frequency control of the resonant converters.

TABLE 2. Comparison of Operating Characteristics at, Below and Above Resonance Operation

	$f_s = f_r$	$f_s < f_r$	$f_s < f_r$
Primary Bridge	ZVS available		potential for ZVS based on dead time
	Low turn-off currents		High turn-off currents
Secondary Bridge	ZCS available from SR		
Losses	Optimized operation and best efficiency	More conduction losses from circulating currents and DCM	Less conduction losses due to CCM
	Unity Gain	ZVS lost if f_s is too low (capacitive region)	High swithcing losses

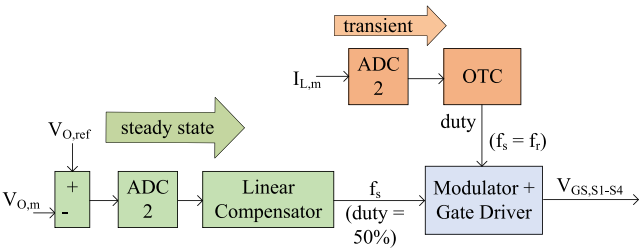

FIGURE 14. OTC control block diagram for an LLC converter.

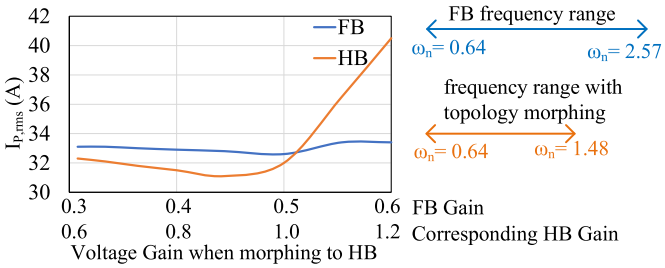

FIGURE 15. Comparison between FB operation and HB morphed operation.

B. OPTIMAL TRAJECTORY CONTROL

When designing a linear compensator for FM, the controllability and/or the accuracy of the controller is limited to around a particular operating point [64], which could be a drawback in wide voltage range applications. In many cases, this is the operating point at which the small signal analysis has been performed. Therefore, nonlinear control techniques based on the graphical state plane analysis (SPA) are proposed for resonant converters. OTC is one such non-linear control technique that was initially proposed for the SRC in [33]. This control technique is supposed to have a lower response time by following a desired trajectory as the control law.

OTC uses SPA. In OTC, the radius of the existing trajectory should be calculated at each operating point based on the estimated values of the state variables i_p and v_{Cr}. When the desired radius is reached, the corresponding switches of the relevant trajectory turn-on, forcing the converter to follow that trajectory. However, as the number of resonant elements or state variables increases, the online calculations on the trajectory become more complicated.

The simplified OTC proposed in [64] uses an FM based linear compensator during the steady state and OTC at transient states. The control block diagram for this is given in Fig. 14.

OTC is applied by changing the pulse width to reach the desired trajectory. Pulse widths are calculated by using the load current to estimate i_p. At $f_s = f_r$, for a step load increase, the radius of the trajectory increases. In order to minimize the transient oscillations at the step change, the trajectory shifts between $f_s < f_r$ and $f_s = f_r$, to facilitate an increase of the trajectory radius in two steps (i.e., the radius increases by one half during one half of the switching cycle, other half during the next half cycle). A similar process is followed for step load decrease. The authors have shown that with simplified OTC integration, the dynamic performance has significantly improved, reducing the output voltage overshoot up to 42% in step load increase and 67% in step load decrease. OTC is preferred to improve the dynamic response, light load efficiency, and soft start [65].

C. TOPOLOGY MORPHING

For extreme voltage ranges, FM will result in wider frequency ranges [66]. Topology morphing techniques are employed for wide input voltage range applications [67], [68], [69]. The voltage gain of the converter can be modified by changing the topology of the primary bridge between the FB and HB, which will reduce the range of operating frequencies in the resonant converters. The gain of the FB is twice that of the HB at fixed input/output voltages. Therefore, FB is used for operation in the high gain region, (i.e., when the output voltage is high and input voltage is low) and HB is used for operation in the low gain region.

Topology morphing is effective in terms of switching loss minimization from f_s reduction, conduction loss minimization, and reduction of the transformer burden from the reduction of the AC root mean square (RMS) current. A simulation based analysis was conducted for a FB CLLC converter with G = [0.3 - 1.2]. It can morph into HB within G = [0.3 - 0.6] (then the effective HB gain will be [0.6 - 1.2]) and operate as FB within G = [0.6 - 1.2]. The comparison of AC RMS currents of the primary bridge ($I_{p,rms}$) and f_s range with and without topology morphing are shown in Fig. 15. Reduction of the AC RMS current is observed when the HB gain is less than 1. Also, it is noted that the AC RMS currents at the same gains of HB and FB are similar, i.e., $I_{p,rms}$ with FB at [G = 1.2] = $I_{p,rms}$ with HB at [G = 1.2] = 40.5 A. Therefore, it is vital to optimize the converter design to maximize efficiency and

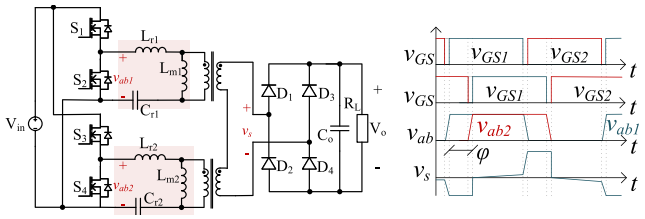

(a) Topology (b) Voltage Waveforms

FIGURE 16. Phase shift control in interleaved LLC converter. (a) Topology. (b) Voltage waveforms.

identify the optimum turns ratio and morphing margin when using topology morphing.

FB can be changed to HB by not switching one leg of the FB, i.e., by keeping the bottom MOSFET continuously on (S_4) and the other off (S_3) [67]. However, abrupt topology transitions will result in transients in the output. Increasing the output filter capacitance significantly will help manage these transients [70]. However, increasing the capacitors will affect the power density and reliability [71].

The strategy proposed in [67] demonstrates a gradual transition between the topologies, giving the control loop sufficient time for close regulation of the output voltage. Here, when morphing from FB to HB, the switching leg continues to be in frequency control and the non-switching leg will be in frequency and duty cycle control. The bottom MOSFETs in the non-switching leg will increase the duty ratio from 0.5 to 1 gradually, while the top MOSFET will decrease the duty ratio from 0.5 to 0 in a complementary manner. However, the transformer core needs to be large enough to avoid saturation due to the asymmetric operation and DC offset currents [68]. The use of OTC for morphing between the topologies is proposed in [69]. Other topology morphing techniques use additional components (i.e., an additional transformer and more switches), which result in added cost and complexity [68].

D. PHASE SHIFT CONTROL

Single, dual, and extended PS control, commonly adopted in DAB converters are also applied to resonant converters, both conventional and derived topologies [72], [73], [74], [75], [76].

In wide voltage range applications, using PS control instead of FM will avoid a wide range of f_s, at the risk of losing ZVS at light loads. The PS control proposed for an interleaved LLC resonant converter given in Fig. 16(a) is presented in [77], ensuring ZVS is preserved. The voltage waveforms of the primary and secondary are also represented in Fig. 16(b), where the phase shift is defined between 2 HBs as φ. The converter operates at fixed $f_s = f_r$.

For the circuit analysis, time domain analysis is used instead of FHA, which is often solved numerically [76], [77]. One of the main advantages of phase shift control in LLC converters is that the impact of L_m and Q-factor on the voltage gain is lesser than that with FM. The work presented in [77] uses trajectories of resonant tank voltage and current to ensure ZVS for the entire operating range. Closed form formulas for voltage gain as a function of phase shift are also derived in the literature [76].

An FM-PS hybrid control for a CLLC converter is proposed in [78], which will result in a narrow range of f_s while realizing ZVS for wide voltage range applications.

IV. RESONANT CONVERTER MODELING TECHNIQUES

A mathematical model of the converter is helpful for design and control optimization and closed loop control development. The modeling technique should be selected based on the application and design criteria. For example, the model should accurately derive the current and voltage stresses for converter optimization. However, a small signal model is required for closed loop control development.

Due to the nonlinear characteristic of resonant converters and higher number of state variables, mathematical modeling is more challenging than DAB converters [79]. This Section reviews the mathematical modeling techniques that can be applied to resonant converters.

A. FHA BASED MODELING

FHA is the simplest modeling technique for resonant converters. It takes into account only the fundamental AC components of voltages and currents of the resonant tank [80]. Equivalent ac load (Req, ac) in Section II is derived based on FHA. However, the accuracy of the model decreases when moving away from f_r. FHA is mostly used to determine resonant tank parameters based on voltage gain functions.

B. LINEARIZED MATHEMATICAL MODEL USING EXTENDED DESCRIBING FUNCTIONS

The concept of extended describing functions (EDFs) was introduced in [81], [82] and [83] to derive the continuous time small signal models in state space representation for resonant converters. State space averaging techniques cannot be used for resonant converters, unlike converters operating with PWM because some state variables in resonant converters do not have DC components, instead carry strong switching frequency harmonics [83].

By using the EDFs, the nonlinear terms of the state space equations of the resonant converter can be approximated either by the fundamental component terms, i.e., $F(x)sin\omega_s t$ or DC terms i.e., $F(x)$, where $F(x)$ is the EDF term. The EDF terms are functions of operating conditions and harmonic coefficients, and they can be evaluated by analyzing the Fourier expansions of the nonlinear terms [81]. EDFs can incorporate any number of harmonics to improve the accuracy of the model. The EDF term at an operating point U_0 can be derived from (20), where k is the harmonic number and x^{ss} is the state vectors at steady state operation.

$$F_k{}^{ss}(X^{ss}, U_0) = \frac{1}{T_s}\int_0^{T_s} f(x^{ss}, U_0, t)e^{-jk\omega_s t}dt \qquad (20)$$

The nonlinear terms in the state space equations of a resonant converter are mostly the primary bridge output voltage (quasi-square voltage), the secondary bridge input voltage, and its output current. EDFs for these are derived in [84] for an HB LLC converter following the procedure described in [83]. EDFs are used to develop small signal models of SRC and PRC in [81] and later are applied to a CLLC converter in [85]. The process of developing the small signal model is summarized below:

- Derive the state space equations for the equivalent circuit of the converter.
- Apply FHA to the sinusoidal voltages and currents in the state space system. (i.e., resonant tank current, voltage across capacitors). This will help to decompose the state space system into Sine, Cosine, and DC terms.
- Apply EDFs to nonlinear terms of the system.
- Apply the averaging operator and linearize the nonlinear terms further by using Taylor series expansion. Each averaged term can be defined as a sum of a steady state term (X) and a perturbation ($\hat{x}$), i.e., $x(t) = X(t) + \hat{x}(t)$

For a perturbation in the control/input variables, the change in response of the output variable is given through the small signal model. The large signal model provides the steady state values of the state variables for a given operating point, hence there are no differential terms of the state variables in the large signal model. The linearized large signal model and small signal model for the LLC or CLLC converter are derived in the form of (21)–(25). $A, B,$ and C are constant matrices/arrays of resonant tank elements and input DC voltage, $\hat{x}$ is an array of small signal state variables, $\hat{u}$ is an array of perturbations in control/input variables (ω_n: normalized switching frequency, v_{in}: input DC voltage, d: duty ratio) and $\hat{y}$ is an array of change in output variables (output DC voltage or current) [85]. Sinusoidal state variables are decomposed into sine and cosine components as denoted by $x_{k,s}$ and $x_{k,c}$, respectively. The fully derived state matrices for an LLC converter and a CLLC converter are given in [86] and [85], respectively.

$$A.X + B.U = 0 \tag{21}$$

$$\frac{d}{dt}\hat{x} = A.\hat{x} + B.\hat{u} \tag{22}$$

$$\hat{y} = C.\hat{x} \tag{23}$$

$$\hat{u} = \begin{bmatrix} \hat{\omega_n} & \hat{v_{in}} & \hat{d} \end{bmatrix}^T \tag{24}$$

$$\hat{x} = \begin{bmatrix} \hat{i_{p,s}} & \hat{i_{p,c}} & \hat{v_{Cr,s}} & \hat{v_{Cr,c}} & \hat{i_{m,s}} & \hat{i_{m,c}} & \hat{v_{Co}} \end{bmatrix}^T \tag{25}$$

The converter model (plant model) can be studied as a function of control variable ω_n (with constant v_{in} and d) to develop the closed loop controller for FM. The process of developing the closed control loop based on the small signal model is presented in detail in [87].

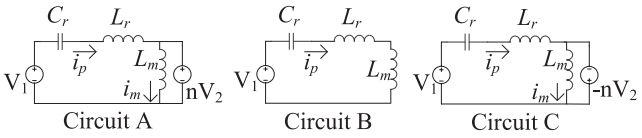

FIGURE 17. Equivalent circuits of LLC converter.

C. TIME DOMAIN MODEL

Time domain modeling for LLC resonant converters is discussed in [88], [89], [90], which can model instantaneous voltages and currents in the equivalent circuit more accurately than frequency domain modeling. Here, it is required to identify the equivalent circuits of the converter for each mode of operation and analyze the circuit under each time interval. Development of the time domain model becomes challenging as the complexity of the resonant converter increases.

The equivalent circuits of the LLC converter in Fig. 5 under FM and SR is given in Fig. 17. With reference to FM waveforms in Fig. 13, equivalent circuit A is applied from t_a to t_b, circuit B is from t_b to t_c, and circuit C is from t_b to t_d. The state space equations are written for each circuit and the functions for AC current (i_p, i_m, i_s) and resonant capacitor voltage (v_{C_r}) are synthesized under different time intervals. The analysis for the LLC converter at $f_s = f_r$ operation (circuit A) is given below. The initial values are given by i_{p0}, i_{m0}, and v_{c0}.

$$i_p(t) = \frac{(-v_{C_r0} + V_{in} - nV_o)}{\omega_r L_r} \sin[\omega_r(t - t_a)] + i_{p0}\cos[w_r(t - t_a)] \tag{26}$$

$$v_{C_r}(t) = (v_{C_r0} - V_{in} + nV_o)\cos[\omega_r(t - t_a)] + \frac{i_{p0}}{\omega_r C_r}\sin[\omega_r(t - t_a)] \tag{27}$$

$$i_m(t) = i_{m0} + \frac{nV_o}{L_m}(t - t_a) \tag{28}$$

$$i_{p0} = i_{m0} = \frac{-nV_o}{4L_m f_s},\ v_{C_r0} = \frac{-\pi^2 L_r f_s I_2}{n} + V_{in} - nV_o \tag{29}$$

The functions for state variables are obtained numerically using tools such as MATLAB. The functions for above and below f_r operation can also be derived similarly.

D. STATE PLANE ANALYSIS

In SPA, the converter is analyzed as a piece-wise linear system under different conduction paths similar to the above mentioned time domain analysis. SPA for resonant converters was introduced in [32], [91] for SRC and PRC. In [64], the authors present the SPA for an LLC converter with a HB at the primary and a center-tapped diode rectifier at the secondary, with six possible linear modes. Similarly, there are three linear modes for the FB LLC converter in Fig. 5 and the CLLC converter in Fig. 8, but with different trajectories due to topological differences. The trajectories also differ based on the switching frequency: $f_s = f_r$, $f_s < f_r$, or $f_s > f_r$.

TABLE 3. Ratings and Parameters of the Resonant TPC

Manufacturer	Input Voltage	Output Voltage	Max. Power	Efficiency	Power Density	Operating frequency	Reference
Texas Instruments	380 - 600 V	280 - 450 V	6.6 kW	98%	2.16 kW/L	300 - 700 kHz	TIDM-02002 [92]
Wolfspeed	380 - 900 V	480 - 800 V	22 kW	98.5%	8 kW/L	135 - 250 kHz	CRD-22DD12N [93]
Wolfspeed	380 - 420 V	400 V	6.6 kW	96%	-	500 - 1000 kHz	CRD-06600DD065N [94]

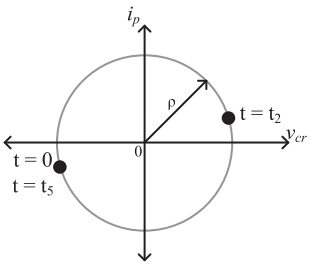

FIGURE 18. Steady state trajectory when $f_s = f_r$.

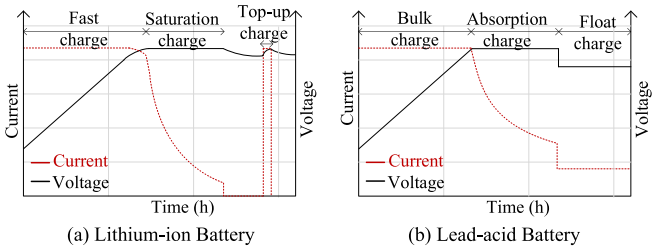

FIGURE 19. Typical battery charging profile.

For the LLC converter in Fig. 5, one linear mode exists at $f_s = f_r$ which switches during $[0 - t_2]$ and $[t_2 - t_5]$. This trajectory is shown in Fig. 18. The radius and center of the trajectory are obtained based on the piece-wise linear analysis of the equivalent circuit for two states: i_p and v_{Cr}. The radius depends on the initial values i_{p0} and v_{C_r0} derived in the previous subsection. The radius of the circle increases with the load.

V. RESONANT CONVERTER DESIGN

This Section explores the application of resonant converters in EVs, typical design parameters in such applications, and practical design considerations of resonant converters.

A. LLC AND CLLC CONVERTERS FOR OBC APPLICATIONS

LLC and CLLC resonant converters are attractive for unidirectional and bidirectional OBC applications, respectively. The most common power ratings of OBCs are 3.3 kW, 6.6 kW, 11 kW, 19.2 kW, and 22 kW [2]. The converter input connects to the PFC stage and the output connects to the HV battery. In 400 V rated batteries, the voltage can vary from 250 V to 450 V; for 800 V rated batteries, it can vary from 550 V to 850 V [2]. Some examples of commercially available bidirectional OBCs are provided in [1]. A comparison among the commercially available CLLC converters for OBCs at or above 6.6 kW power rating is provided in Table 3. All the presented configurations use silicon carbide (SiC) MOSFETs and are air-cooled.

The battery charging profile should be considered when designing and modeling power converters and their controllers for charger applications. Typical battery charging profiles of a Lithium-ion battery and a Lead-acid battery are shown in Fig. 19 [95], [96]. It can be observed that both batteries have constant current (CC) and constant voltage (CV) modes.

Typical features of Lithium-ion batteries for EV applications can be summarized as below:

- Preferred for HV batteries (400 V and above)
- Typical open circuit voltage (OCV) is 2.5 V (fully depleted) to 4.2 V (fully charged) per cell (hence typical voltage swing for 400 V battery is 250 V to 450 V) [96]
- Charging time is faster than Lead-acid batteries [95]

Typical features of Lead-acid batteries for EV applications can be summarized as below:

- Preferred for 12 V and 48 V batteries
- Typical OCV is 1.8 V (fully depleted) to 2.1 V (fully charged) per cell (lower voltage swing compared to Lithium-ion batteries) [97]
- comparatively slow charging time

LLC converter design for Lead-acid and Lithium-ion batteries are presented in [98] and [18], respectively. Additionally, there is a trickle charging stage before the CC stage for fully depleted batteries, where the cells are charged with a constant current of 10% of the maximum current [18], [88].

In the CC stage, the constant charging current or charging rate (C-rate) can have multiple levels as limited by the maximum rated power of the converter [18]. OBC operating points can be identified by analyzing the charging profile of the battery pack so that the converter can be optimized for the

desired operating region. Based on the battery charger profile, the full load operation may occur at the CC stage, and not at maximum gain (maximum output voltage). However, OBC manufacturers try to maintain a constant maximum power throughout the charging profile at minimum input voltage due to diverse battery charging profiles [18].

When using resonant converters in OBC applications, the Q-factor at the worst case operating point needs to be identified. In [18], for an LLC converter, the authors have derived formulas in (30) and (31) to obtain the Q-factor at constant maximum power charging (Q_{CMP}) and at maximum gain ($Q_{G,\max}$) in the inductive region, and used those along with the h-ratio to develop a constraint to find the optimum design with minimum circulating currents.

$$Q_{CMP}(Z_0, M) = \frac{\pi^2}{8}\frac{P_{out,\max}}{GV_{in,\max}}Z_0 \tag{30}$$

$$Q_{G,max}(h, M) = \frac{1}{hG}\sqrt{h + \frac{G^2}{G^2 - 1}} \tag{31}$$

B. RESONANT CONVERTER OPTIMIZATION

The resonant converter design includes determining the resonant tank (series resonant inductor, capacitor, and transformer magnetizing inductor for an LLC converter), transformer turns ratio and range of switching frequency f_s. These values cannot be selected arbitrarily. With the use of the converter characteristic functions in (11)–(15), the optimum converter design parameters can be evaluated for maximum efficiency and power density.

The work on resonant converter optimization is still improving. There are a few literature sources discussing the resonant converter optimization with room for improvement, when accommodating wide input and output voltage ranges, and different modes of converter operation [88], [89], [90], [99], [100]. The objective of the converter optimization is to determine optimum converter parameters to maximize the efficiency and/or power density, such that the constraints relevant to the successful operation of the converter throughout the desired operating region are met.

In resonant converters for battery charger applications, maximization of the weighted average efficiency for the entire battery charging profile can be set as an optimization objective. In [88], a time weighted average efficiency (TWAE) based on the instantaneous efficiency and the state of charge (SOC) is defined to formulate the optimization objective function. The proposed optimization procedure is summarized in Fig. 20 for a frequency controlled LLC converter.

The converter is modeled based on the time domain as discussed in Section IV. The authors have used variable-step exhaustive search algorithm to find the optimum resonant tank parameters. However, this optimization procedure can be further improved to find the optimum transformer turns ratio and reach multi objectives, such as power density maximization.

The LLC converter model derived based on different methods discussed in Section IV, should consider the different

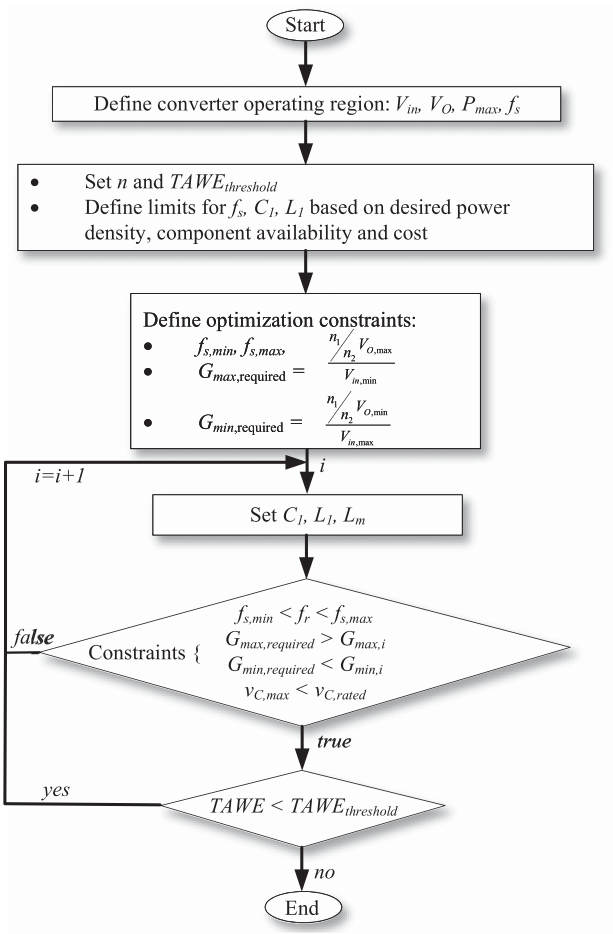

FIGURE 20. Optimal design methodology for an LLC converter.

modes of operation of the converter under frequency control to apply for converter optimization. Due to the nonlinearity of the model, the objective function and the constraints are challenging to solve as they do not have a closed form solution. In [100], a mode solver is proposed to solve the steady state model of an LLC converter. The optimization variables also include transformer turns ratio and full-load switching frequency in addition to resonant tank parameters. The mode solver is derived from the steady state analysis, and instead of pre-determining the mode of operation, all modes are modeled. Based on the optimization variable values, the operation mode is determined and numerical nonlinear programming is used to solve the model. The current and voltage waveforms from the mode solver are then used to model the converter losses and calculate the converter efficiency. However, the optimization objective is limited to maximizing full-load efficiency and constraints with respect to wide voltage and power range operation are not considered.

C. DESIGN CONSIDERATIONS

Following the determination of optimum design parameters, additional factors need to be considered to ensure optimal converter operation. Major factors are discussed below.

1) COMPONENT SELECTION AND TOLERANCES

In MOSFET selection, dv/dt turn-on limits, diode reverse recovery, and losses should be considered [98]. In resonant converters with soft switching, conduction losses will be dominating, hence switches with lower on-state resistance should be selected. Multi layer ceramic capacitors (MLCC) are preferred for resonant capacitors due to stable capacitance, tight tolerances, and low energy dissipation [101].

While determining converter design parameters, tolerances of the resonant tank components should be investigated to ensure the converter operation for the entirety of the operating voltage and power range. The typical tolerance values can be included in the optimization process.

2) TRANSFORMER DESIGN

The high frequency transformer in the converter provides galvanic isolation between primary and secondary sides, and steps up or down the voltage based on the turns ratio [102]. The design of the high frequency isolation transformer is critical, because it is one of the main contributors to the converter weight and volume, and particularly in resonant converters because of the restricted magnetizing inductance and parasitics [103]. Planar transformers with printed circuit board (PCB) or Litz wire windings are preferred over conventional wire-wound transformers because of their advantages in terms of low profile, good thermal characteristics, high power density, repeatability, modularity, and ease of manufacturing [104]. However, there are certain limitations in planar transformers as well, such as large surface area and high intertwining (parasitic) capacitance (can be predicted) [104]. Planar transformers with PCB windings, even though easier to make, has the concern of a limited number of turns (hence the need to connect transformers in series). Therefore, it is important to optimize the transformer design to achieve the converter design objectives.

In LLC converter applications, efforts are being made to partial or full integrate the series resonant tank into the transformer [105], [106], [107], [108]. The desired L_m can be realized by introducing an air gap to the transformer core [109]. As proposed in [110] and [111], series resonant tank can reside fully or partially in a separate core and connected to the top or side of the planar transformer. The design process is relatively simpler as L_r and L_m have their own flux paths [112]. An improved integrated transformer design with reduced volume is proposed in [113] by introducing the series resonant tank (L_r, C_r) as a magnetic insertion between the primary and secondary windings. The magnetic insertion consists of a dielectric substrate with conductor windings directly deposited on both sides.

3) PARASITIC ANALYSIS

Resonant converters are sensitive to parasitics, mainly introduced by the transformer as inter-winding and intra-winding capacitance and PCBs. Hence, analyzing the transformer parasitics during the design stage is important. A comprehensive process to calculate the parasitic capacitance in the transformer is provided in [114]. Calculations for a static capacitance model are provided considering layer-to-layer capacitance.

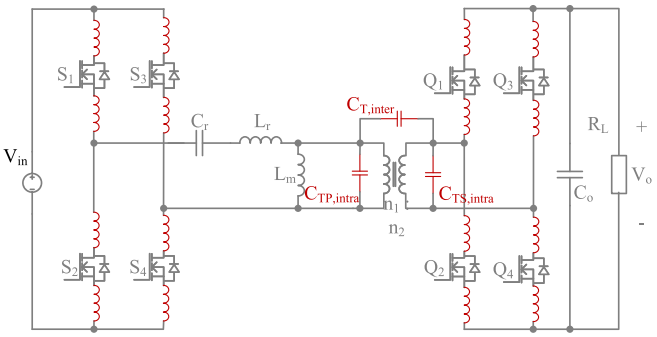

FIGURE 21. Parasitic components in an LLC converter.

The parasitic model for a resonant converter discussed in [115] is demonstrated in Fig. 21. These parasitics cause ringing in the transformer voltage and current and deviations in the gain characteristic [115], [116]. The effect of parasitics increases with decreasing load [116].

Methods of reducing the parasitic effects in planar transformers with PCB windings are proposed in [115], [116], [117]. The total static inter-winding capacitance can be reduced by reducing the number of primary-secondary intersections and permittivity of the insulation material between layers [116]. However, reducing the number of primary-secondary intersections will increase the AC-DC resistance ratio in the transformer. Hence, the trade-off must be considered [116]. In [115], high parasitic capacitance calling for increased dead band is investigated, and as a solution, reducing the resonant capacitance is proposed.

D. DEAD TIME EVALUATION

Dead time is the duration in which both the MOSFETs in a leg are off. When selecting the dead time, the designer must be mindful of MOSFET switching times as they vary based on the MOSFET technology: WBG or silicon (Si) MOSFETs. As discussed in Section III, dead time should be long enough to facilitate ZVS and short enough to minimize the diode forward conduction loss during zero power transfer. Hence, optimum dead time evaluation is important to minimize the converter losses.

Minimum dead time can be evaluated as the dead time required to achieve ZVS in the worst case, at light or no load conditions [118]. In [119], a time domain analysis is used to derive a closed form solution for minimum dead time. Also, for resonant converters with FM, $t_d << 1/f_{s,max}$ [119].

However, selecting $t_{d,\min}$ based on ZVS in the worst case may lead to excess dead time. Hence, resulting in high diode conduction losses at medium and heavy loads. Hence, [120] highlights the importance of an adaptive dead time strategy as already used in commercial resonant controllers from ON

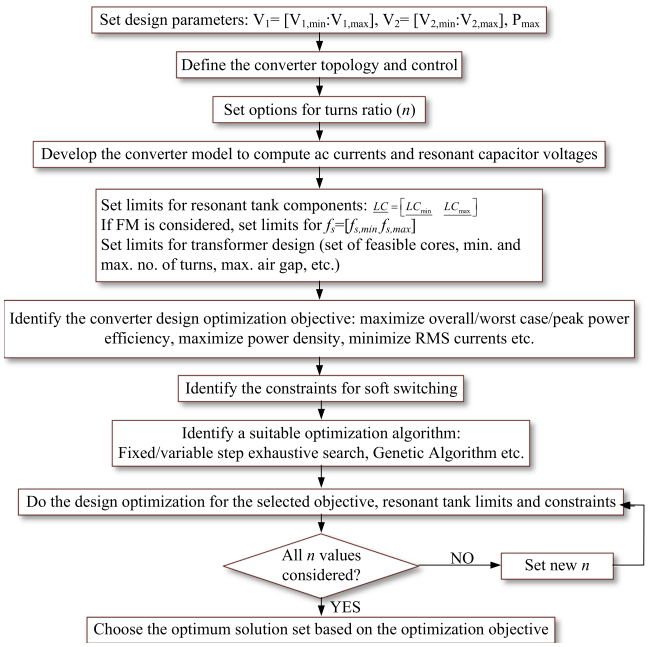

FIGURE 22. Proposed generalized structure for resonant converter optimization.

Semiconductor, Texas Instruments, and STMicroelectronics. In this strategy, a dv/dt detector can be used to identify ZVS operation, and the relevant MOSFET is turned on following the identification. However, WBG devices can have a high dv/dt, which may introduce noise during ZVS detection. Therefore, a time domain analysis based adaptive dead time strategy is presented in [120] and around 1% efficiency improvement is achieved.

VI. POTENTIAL RESEARCH DIRECTIONS AND FUTURE PROSPECTS

During this literature review on voltage source DC-DC resonant converters, following gaps in research and future prospects were identified.

A. TOPOLOGICAL IMPROVEMENTS

The main advantages of using a resonant tank in voltage source DC-DC converters are sinusoidal current waveforms and soft switching availability. Novel resonant converter topologies are being derived based on conventional topologies to meet the evolving demands of EV applications. The DC-DC converters for EV applications are now exploring HV and high power domain, especially for DC fast charging (> 1 kV and ≈ 900 kW) [121]. Interleaved resonant converters discussed in Section II have the potential to be used in high power applications by interleaving bridges for current sharing. However, meeting HV requirements is a challenge as the voltage rating of the commercially available MOSFETs is limited to 1.7–2 kV, limiting the converter rating to a maximum of 1 kV [122]. Hence, using 3 L or 5 L NPC arms in interleaved resonant converters makes it a promising candidate for HV and high power applications.

B. RESONANT CONVERTER CONTROL

New hybrid control techniques for DC-DC resonant converters are published frequently in the literature to address wide voltage range applications, transients, and soft switching. However, limited literature includes the closed loop control implementation of these hybrid techniques, which is equally important. Discretized closed loop control has significant impacts from delays and quantization noise from filters which must be modeled and checked for stability along with the closed loop compensation.

C. CONVERTER MODELING

With the topological and control improvements, and increase in resonant components, progress in mathematical modeling of resonant converters, even though challenging, is inevitable. The availability of computational tools like MATLAB can aid in solving the converter models to obtain numerical solutions.

1) HARMONIC STATE SPACE MODEL

The harmonic state space (HSS) model is an extension to the FHA based state space model given in (22)–(25) above [123]. Literature on this technique applied to DC-DC resonant converters are scarce, but it can improve the accuracy of the model in wide voltage range applications. In HSS model, each state variable is written as the sum of harmonics instead of considering only the first harmonic as given in (32) [124]. Each harmonic of the state variable can be expanded as in (33)–(36).

$$x(t) = \sum_{k\epsilon\mathbb{Z}} X_k e^{jk\omega_1 t} \tag{32}$$

$$s\mathbf{X} = (\mathbf{A} - \mathbf{Q})\mathbf{X} + \mathbf{BU} \tag{33}$$

$$\mathbf{X} = [X_{-h}, \ldots, X_{-1}, X_0, X_1, \ldots, X_h]^T \tag{34}$$

$$\mathbf{U} = [U_{-h}, \ldots, U_{-1}, U_0, U_1, \ldots, U_h]^T \tag{35}$$

$$\mathbf{A} = \begin{bmatrix} A_0 & \ldots & A_{-h} & & \\ \vdots & \ddots & \ddots & & \\ A_h & \ddots & A_0 & \ddots & A_{-h} \\ & \ddots & \ddots & \ddots & \vdots \\ & & A_h & \ldots & A_0 \end{bmatrix} \tag{36}$$

2) SPACE MAPPING TECHNIQUE

In order to bridge the gap between less accurate mathematical model (coarse model) and the actual converter prototype or simulation model (fine model), space mapping is a promising technique [125], [126]. A mapping between the coarse model and fine model is created to obtain the surrogate model, which is more accurate than the coarse model but has lesser computation time/burden than the fine model.

3) POLYTOPIC MODEL

Polytopic modeling is another approach which can be applied to comprehensive resonant topologies where time domain modeling cannot be applied. Here, the converter is modeled as a black box and the input parameters are mapped to the output parameters as a linear or a nonlinear system [127]. A simulation model in a spice tool or PLECS can aid in creating the mapping.

D. CONVERTER DESIGN

The main research gap in terms of resonant converter design is design optimization. The existing literature on this mainly focus on LLC and CLLC design optimization, with limitations as discussed in Section V above. While new topologies are being derived, it is also essential to discuss their design optimization. A proposed structure for design optimization that can be adapted to any topology is given in Fig. 22. This would also require a sufficiently accurate model of the converter. This proposed structure, even though highly ideal in nature, sufficiently presents expectations of the resonant converter design optimization.

VII. CONCLUSION

This paper presents the design, control, and modeling of resonant converters for EV applications and can be used as a guide for DC-DC voltage source resonant converter design. The basic and conventional voltage source resonant converter topologies: SRC, PRC, SPRC, and LLC topologies, are discussed. New topologies derived in the form of reconfigurable, hybrid, and interleaved resonant converters have also been reviewed and compared. When moving into HV and high power domain interleaved hybrid resonant topologies are promising.

FM, PS, OTC, and topology morphing are identified and reviewed as resonant converter control techniques. FM is the classical control technique for resonant converters, which can ensure soft switching. However, wide voltage range applications can lead to a wide range of switching frequencies, affecting the converter efficiency. PS control and topology morphing between FB and HB are advantageous in such applications. OTC developed based on the SPA is improves the dynamic response during transients.

Mathematical models of resonant converters are important for converter design and control. FHA model, linearized model using EDFs, time domain model, and SPA are discussed. EDF based models are used for small signal analysis in closed loop control design and time domain modeling is preferred in design or control optimization.

This paper also discusses resonant converter design optimization along with design considerations such as battery charging profile, component selection, and isolation transformer design. There are potential research opportunities in resonant converter topological improvements, design and control optimization of resonant converters for HV, high power, and wide input/output voltage range EV applications.

REFERENCES

[1] J. Yuan, L. Dorn-Gomba, A. D. Callegaro, J. Reimers, and A. Emadi, "A review of bidirectional on-board chargers for electric vehicles," *IEEE Access*, vol. 9, pp. 51501–51518, 2021.

[2] H. K. Bai et al., "Charging electric vehicle batteries: Wired and wireless power transfer: Exploring EV charging technologies," *IEEE Power Electron. Mag.*, vol. 9, no. 2, pp. 14–29, Jun. 2022.

[3] N. Keshmiri, D. Wang, B. Agrawal, R. Hou, and A. Emadi, "Current status and future trends of GaN HEMTs in electrified transportation," *IEEE Access*, vol. 8, pp. 70553–70571, 2020.

[4] *SAE Electric Vehicle and Plug in Hybrid Electric Vehicle Conductive Charge Coupler J1772-201710*, Standard J1772_201710, SAE International, Warrendale, PA, USA, 2017. Accessed: Jul. 14, 2022. [Online]. Available: https://www.sae.org/standards/content/j1772_201710/

[5] Wikipedia.com, "Charging station," 2023. Accessed: Sep. 26, 2023. [Online]. Available: https://en.wikipedia.org/wiki/Charging_station

[6] J. M. Gitlin, "You won't be confused about electric vehicle charging after reading this," 2022. Accessed: Sep. 26, 2023. [Online]. Available: https://arstechnica.com/cars/2022/07/the-ars-technica-guide-to-electric-vehicle-charging/3/

[7] Inside Evs, "SAE releases charging standard for big rigs/trucks," 2018. Accessed: Sep. 19, 2022. [Online]. Available: https://insideevs.com/news/338123/sae-releases-charging-standard-for-big-rigs-trucks/

[8] P. He and A. Khaligh, "Comprehensive analyses and comparison of 1 kW isolated DC–DC converters for bidirectional EV charging systems," *IEEE Trans. Transp. Electrific.*, vol. 3, no. 1, pp. 147–156, Mar. 2016.

[9] H. Qin and J. W. Kimball, "Generalized average modeling of dual active bridge DC–DC converter," *IEEE Trans. Power Electron.*, vol. 27, no. 4, pp. 2078–2084, Apr. 2012.

[10] B. Zhao, Q. Yu, and W. Sun, "Extended-phase-shift control of isolated bidirectional DC–DC converter for power distribution in microgrid," *IEEE Trans. Power Electron.*, vol. 27, no. 11, pp. 4667–4680, Nov. 2012.

[11] H. Huang, "Designing an LLC resonant half-bridge power converter," in *Proc. Texas Instrum. Power Supply Des. Seminar*, 2010, pp. 2010–2011.

[12] K. Siebke and R. Mallwitz, "Comparison of a dual active bridge and CLLC converter for on-board vehicle chargers using GAN and time domain modeling method," in *Proc. IEEE Energy Convers. Congr. Expo.*, 2020, pp. 1210–1216.

[13] S. Deshmukh et al., "Review on classification of resonant converters for electric vehicle application," *Energy Rep.*, vol. 8, pp. 1091–1113, 2022.

[14] N. Mohan, T. M. Undeland, and W. P. Robbins, *Power Electronics: Converters, Applications, and Design*. Hoboken, NJ, USA: Wiley, 2003.

[15] M. Yano, M. Matsui, T.-H. Chin, K. Kuroki, and T. Shimizu, "Recent trends in power conversions," in *Proc. 26th Annu. Conf. IEEE Ind. Electron. Soc. IEEE Int. Conf. Ind. Electron., Control Instrum. 21st Century Technol.*, 2000, pp. 1340–1346.

[16] R. King and T. Stuart, "A normalized model for the half-bridge series resonant converter," *IEEE Trans. Aerosp. Electron. Syst.*, vol. AES-17, no. 2, pp. 190–198, Mar. 1981.

[17] M. K. Kazimierczuk and D. Czarkowski, *Resonant Power Converters*. Hoboken, NJ, USA: Wiley, 2012.

[18] J. Deng, S. Li, S. Hu, C. C. Mi, and R. Ma, "Design methodology of LLC resonant converters for electric vehicle battery chargers," *IEEE Trans. Veh. Technol.*, vol. 63, no. 4, pp. 1581–1592, May 2014.

[19] P. K. Jain, A. St-Martin, and G. Edwards, "Asymmetrical pulse-width-modulated resonant DC/DC converter topologies," *IEEE Trans. Power Electron.*, vol. 11, no. 3, pp. 413–422, May 1996.

[20] J.-W. Kim and P. Barbosa, "PWM-controlled series resonant converter for universal electric vehicle charger," *IEEE Trans. Power Electron.*, vol. 36, no. 12, pp. 13578–13588, Dec. 2021.

[21] C. Bai, B. Han, B.-H. Kwon, and M. Kim, "Highly efficient bidirectional series-resonant DC/DC converter over wide range of battery voltages," *IEEE Trans. Power Electron.*, vol. 35, no. 4, pp. 3636–3650, Apr. 2020.

[22] P. A. Thollot, *Power Electronics Technology and Applications 1993*. New York City, NY, USA: IEEE, 1992.

[23] S.-H. Ryu, D.-H. Kim, M.-J. Kim, J.-S. Kim, and B.-K. Lee, "Adjustable frequency– duty-cycle hybrid control strategy for full-bridge series resonant converters in electric vehicle chargers," *IEEE Trans. Ind. Electron.*, vol. 61, no. 10, pp. 5354–5362, Oct. 2014.

[24] S. Habib et al., "Contemporary trends in power electronics converters for charging solutions of electric vehicles," *CSEE J. Power Energy Syst.*, vol. 6, no. 4, pp. 911–929, Dec. 2020.

[25] P. C. Todd and R. W. Lutz, "A practical parallel loaded resonant power supply," in *Proc. IEEE Appl. Power Electron. Conf. Expo.*, 1986, pp. 90–97.

[26] Y.-G. Kang and A. K. Upadhyay, "Analysis and design of a half-bridge parallel resonant converter," in *Proc. IEEE Power Electron. Specialists Conf.*, 1987, pp. 231–243.

[27] J. Bu, M. Sznaier, Z.-Q. Wang, and I. Baterseh, "Robust controller design for a parallel resonant converter using/spl mu/-synthesis," *IEEE Trans. Power Electron.*, vol. 12, no. 5, pp. 837–853, Sep. 1997.

[28] R. L. Steigerwald, "A comparison of half-bridge resonant converter topologies," *IEEE Trans. Power Electron.*, vol. 3, no. 2, pp. 174–182, Apr. 1988.

[29] S. Shah and A. K. Upadhyay, "Analysis and design of a half-bridge series-parallel resonant converter operating in discontinuous conduction mode," in *Proc. 5th Annu. Proc. Appl. Power Electron. Conf. Expo.*, 1990, pp. 165–174.

[30] V. Vorperian and S. Cuk, "A complete DC analysis of the series resonant converter," in *Proc. IEEE Power Electron. Specialists Conf.*, 1982, pp. 85–100.

[31] J.-W. Gong, S.-H. Ahn, H.-J. Ryoo, and S.-R. Jang, "Comparison of DCM and CCM operated resonant converters for high-voltage capacitor charger," in *Proc. 39th Annu. Conf. IEEE Ind. Electron. Soc.*, 2013, pp. 532–537.

[32] R. Oruganti and F. C. Lee, "Resonant power processors, Part II—Methods of control," *IEEE Trans. Ind. Appl.*, vol. IA-21, no. 6, pp. 1461–1471, Nov. 1985.

[33] R. Oruganti, J. J. Yang, and F. C. Lee, "Implementation of optimal trajectory control of series resonant converter," *IEEE Trans. Power Electron.*, vol. 3, no. 3, pp. 318–327, Jul. 1988.

[34] R. Oruganti and T. C. How, "Resonant-tank control of parallel resonant converter," *IEEE Trans. Power Electron.*, vol. 8, no. 2, pp. 127–134, Apr. 1993.

[35] MathWorks, "Robust controller design using Mu synthesis," 2023. Accessed: Feb. 20, 2023. [Online]. Available: https://www.mathworks.com/help/robust/ug/robust-controller-design-using-mu-synthesis.html

[36] M. K. Kazimierczuk, N. Thirunarayan, and S. Wang, "Analysis of series-parallel resonant converter," *IEEE Trans. Aerosp. Electron. Syst.*, vol. 29, no. 1, pp. 88–99, Jan. 1993.

[37] C. Lee, S. Sooksatra, and R. Liu, "Constant frequency controlled full-bridge LCC-type parallel resonant converter," in *Proc. 6th Annu. Appl. Power Electron. Conf. Exhib.*, 1991, pp. 587–593.

[38] H. Chen, E. K. K. Sng, and K.-J. Tseng, "Generalized optimal trajectory control for closed loop control of series-parallel resonant converter," *IEEE Trans. Power Electron.*, vol. 21, no. 5, pp. 1347–1355, Sep. 2006.

[39] X. Tang, Y. Xing, H. Wu, and J. Zhao, "An improved LLC resonant converter with reconfigurable hybrid voltage multiplier and PWM-Plus-PFM hybrid control for wide output range applications," *IEEE Trans. Power Electron.*, vol. 35, no. 1, pp. 185–197, Jan. 2020.

[40] D. Shu and H. Wang, "An ultrawide output range LLC resonant converter based on adjustable turns ratio transformer and reconfigurable bridge," *IEEE Trans. Ind. Electron.*, vol. 68, no. 8, pp. 7115–7124, Aug. 2021.

[41] I.-O. Lee, "Hybrid PWM-resonant converter for electric vehicle on-board battery chargers," *IEEE Trans. Power Electron.*, vol. 31, no. 5, pp. 3639–3649, May 2016.

[42] J. Wu, S. Li, S.-C. Tan, and S. Y. R. Hui, "Fixed-frequency phase-shift modulated capacitor-clamped LLC resonant converter for EV charging," *IEEE Trans. Power Electron.*, vol. 37, no. 11, pp. 13730–13742, Nov. 2022.

[43] K. Jin and X. Ruan, "Hybrid full-bridge three-level LLC resonant converter—A novel DC–DC converter suitable for fuel-cell power system," *IEEE Trans. Ind. Electron.*, vol. 53, no. 5, pp. 1492–1503, Oct. 2006.

[44] Y. Xuan, X. Yang, W. Chen, T. Liu, and X. Hao, "A novel three-level CLLC resonant DC–DC converter for bidirectional EV charger in DC microgrids," *IEEE Trans. Ind. Electron.*, vol. 68, no. 3, pp. 2334–2344, Mar. 2021.

[45] Z. Zhang, T. Jin, X. Xiao, W. Wu, and Y. Yuan, "A novel bidirectional five-level multimode CLLC resonant converter," *IEEE Trans. Power Electron.*, vol. 37, no. 6, pp. 6972–6985, Jun. 2022.

[46] X. Zhou et al., "A high-efficiency high-power-density on-board low-voltage DC–DC converter for electric vehicles application," *IEEE Trans. Power Electron.*, vol. 36, no. 11, pp. 12781–12794, Nov. 2021.

[47] M. I. Shahzad, S. Iqbal, and S. Taib, "Interleaved LLC converter with cascaded voltage-doubler rectifiers for deeply depleted PEV battery charging," *IEEE Trans. Transp. Electrific.*, vol. 4, no. 1, pp. 89–98, Mar. 2018.

[48] G. Yang, P. Dubus, and D. Sadarnac, "Double-phase high-efficiency, wide load range high-voltage/low-voltage LLC DC/DC converter for electric/hybrid vehicles," *IEEE Trans. Power Electron.*, vol. 30, no. 4, pp. 1876–1886, Apr. 2015.

[49] H. Wu, X. Zhan, and Y. Xing, "Interleaved LLC resonant converter with hybrid rectifier and variable-frequency plus phase-shift control for wide output voltage range applications," *IEEE Trans. Power Electron.*, vol. 32, no. 6, pp. 4246–4257, Jun. 2017.

[50] Z. Hu, Y. Qiu, L. Wang, and Y.-F. Liu, "An interleaved LLC resonant converter operating at constant switching frequency," *IEEE Trans. Power Electron.*, vol. 29, no. 6, pp. 2931–2943, Jun. 2014.

[51] Z. Hu, Y. Qiu, Y.-F. Liu, and P. C. Sen, "A control strategy and design method for interleaved LLC converters operating at variable switching frequency," *IEEE Trans. Power Electron.*, vol. 29, no. 8, pp. 4426–4437, Aug. 2014.

[52] Y. Chen, J. Xu, Y. Gao, L. Lin, J. Cao, and H. Ma, "Analysis and design of phase-shift pulse-frequency-modulated full-bridge LCC resonant converter," *IEEE Trans. Ind. Electron.*, vol. 67, no. 2, pp. 1092–1102, Feb. 2020.

[53] J. Deng, C. C. Mi, R. Ma, and S. Li, "Design of LLC resonant converters based on operation-mode analysis for level two PHEV battery chargers," *IEEE/ASME Trans. Mechatronics*, vol. 20, no. 4, pp. 1595–1606, Aug. 2015.

[54] J. Min and M. Ordonez, "Bidirectional resonant CLLC charger for wide battery voltage range: Asymmetric parameters methodology," *IEEE Trans. Power Electron.*, vol. 36, no. 6, pp. 6662–6673, Jun. 2021.

[55] J. F. Lazar and R. Martinelli, "Steady-state analysis of the LLC series resonant converter," in *Proc. 16th Annu. IEEE Appl. Power Electron. Conf. Expo.*, 2001, pp. 728–735.

[56] J.-H. Jung, H.-S. Kim, M.-H. Ryu, and J.-W. Baek, "Design methodology of bidirectional CLLC resonant converter for high-frequency isolation of DC distribution systems," *IEEE Trans. Power Electron.*, vol. 28, no. 4, pp. 1741–1755, Apr. 2013.

[57] S. Zou, J. Lu, A. Mallik, and A. Khaligh, "3.3 kW CLLC converter with synchronous rectification for plug-in electric vehicles," in *Proc. IEEE Ind. Appl. Soc. Annu. Meeting*, 2017, pp. 1–6.

[58] N. Chen et al., "A synchronous rectification scheme based on inductor voltage sensing for CLLC bidirectional resonant converter," in *Proc. IEEE Appl. Power Electron. Conf. Expo.*, 2020, pp. 1713–1719.

[59] Y. Wei, Q. Luo, and H. A. Mantooth, "Synchronous rectification for LLC resonant converter: An overview," *IEEE Trans. Power Electron.*, vol. 36, no. 6, pp. 7264–7280, Jun. 2021.

[60] Toshiba Electronic Devices & Storage Corporation, "Power MOSFET electrical characteristics," 2023. Accessed: Aug. 6, 2022. [Online]. Available: https://toshiba.semicon-storage.com/info/docget.jsp?did=13415

[61] U. Kundu, K. Yenduri, and P. Sensarma, "Accurate ZVS analysis for magnetic design and efficiency improvement of full-bridge LLC resonant converter," *IEEE Trans. Power Electron.*, vol. 32, no. 3, pp. 1703–1706, Mar. 2017.

[62] Y. Gu, Z. Lu, L. Hang, Z. Qian, and G. Huang, "Three-level LLC series resonant DC/DC converter," *IEEE Trans. Power Electron.*, vol. 20, no. 4, pp. 781–789, Jul. 2005.

[63] I.-O. Lee and G.-W. Moon, "Analysis and design of a three-level LLC series resonant converter for high-and wide-input-voltage applications," *IEEE Trans. Power Electron.*, vol. 27, no. 6, pp. 2966–2979, Jun. 2012.

[64] W. Feng, F. C. Lee, and P. Mattavelli, "Simplified optimal trajectory control (SOTC) for LLC resonant converters," *IEEE Trans. Power Electron.*, vol. 28, no. 5, pp. 2415–2426, May 2013.

[65] CPES VT, "Optimal trajectory controls for LLC resonant converters," 2013. Accessed: Mar. 8, 2023. [Online]. Available: https://www.youtube.com/watch?v=Kd756pnElkc

[66] H. Pinheiro, P. K. Jain, and G. Joós, "Self-sustained oscillating resonant converters operating above the resonant frequency," *IEEE Trans. Power Electron.*, vol. 14, no. 5, pp. 803–815, Sep. 1999.

[67] M. M. Jovanović and B. T. Irving, "On-the-fly topology-morphing control—Efficiency optimization method for LLC resonant converters operating in wide input-and/or output-voltage range," *IEEE Trans. Power Electron.*, vol. 31, no. 3, pp. 2596–2608, Mar. 2016.

[68] Y. Wei, Q. Luo, and H. A. Mantooth, "A novel LLC converter with topology morphing control for wide input voltage range application," *IEEE Trans. Emerg. Sel. Topics Power Electron.*, vol. 10, no. 2, pp. 1563–1574, Apr. 2022.

[69] D. Sha and X. Yang, "Wide voltage input full bridge (FB)/Half bridge (HB) morphing based LLC DC–DC converter using numerical optimal trajectory control," *IEEE Trans. Ind. Electron.*, vol. 70, no. 4, pp. 3697–3707, Apr. 2023.

[70] H. Hu, X. Fang, F. Chen, Z. J. Shen, and I. Batarseh, "A modified high-efficiency LLC converter with two transformers for wide input-voltage range applications," *IEEE Trans. Power Electron.*, vol. 28, no. 4, pp. 1946–1960, Apr. 2013.

[71] D. Girling, "Capacitors: Reliability, life and the relevance on circuit design," *Microelectronics Rel.*, vol. 6, no. 1, pp. 35–51, 1967.

[72] Z. Guo and M. Li, "An optimized DPS control strategy for LCL resonant dual active bridge converter for wide voltage conversion ratio," *IEEE J. Emerg. Sel. Topics Ind. Electron.*, vol. 2, no. 4, pp. 501–512, Oct. 2021.

[73] M. Yaqoob, K. Loo, and Y. M. Lai, "A four-degrees-of-freedom modulation strategy for dual-active-bridge series-resonant converter designed for total loss minimization," *IEEE Trans. Power Electron.*, vol. 34, no. 2, pp. 1065–1081, Feb. 2019.

[74] K. Murata and F. Kurokawa, "An interleaved PFM LLC resonant converter with phase-shift compensation," *IEEE Trans. Power Electron.*, vol. 31, no. 3, pp. 2264–2272, Mar. 2016.

[75] H. Wu, T. Mu, X. Gao, and Y. Xing, "A secondary-side phase-shift-controlled LLC resonant converter with reduced conduction loss at normal operation for hold-up time compensation application," *IEEE Trans. Power Electron.*, vol. 30, no. 10, pp. 5352–5357, Oct. 2015.

[76] X. Sun, X. Li, Y. Shen, B. Wang, and X. Guo, "Dual-bridge LLC resonant converter with fixed-frequency PWM control for wide input applications," *IEEE Trans. Power Electron.*, vol. 32, no. 1, pp. 69–80, Jan. 2017.

[77] B. Xue, H. Wang, J. Liang, Q. Cao, and Z. Li, "Phase-shift modulated interleaved LLC converter with ultrawide output voltage range," *IEEE Trans. Power Electron.*, vol. 36, no. 1, pp. 493–503, Jan. 2021.

[78] A. V. Mirtchev and E. C. Tatakis, "Design methodology based on dual control of a resonant dual active bridge converter for electric vehicle battery charging," *IEEE Trans. Veh. Technol.*, vol. 71, no. 3, pp. 2691–2705, Mar. 2022.

[79] V. R. Vakacharla, A. K. Rathore, P. R. Tripathi, and R. K. Keshri, "A comprehensive review of fundamental harmonic approximation analysis techniques for series-parallel resonant converters with capacitive filter," in *Proc. 45th Annu. Conf. IEEE Ind. Electron. Soc.*, 2019, pp. 2581–2585.

[80] M. Rezayati, F. Tahami, J.-L. Schanen, and B. Sarrazin, "Generalized state-plane analysis of bidirectional CLLC resonant converter," *IEEE Trans. Power Electron.*, vol. 37, no. 5, pp. 5773–5785, May 2022.

[81] E. X. Yang, F. C. Lee, and M. M. Jovanovic, "Small-signal modeling of series and parallel resonant converters," in *Proc. IEEE Ann. Appl. Power Electron. Conf. Expo.*, 1992, pp. 785–792.

[82] E. X. Yang, F. C. Lee, and M. M. Jovanovic, "Small-signal modeling of LCC resonant converter," in *Proc. 23rd Annu. IEEE Power Electron. Specialists Conf.*, 1992, pp. 941–948.

[83] E. X.-Q. Yang, "Extended describing function method for small-signal modeling of resonant and multi-resonant converters," Ph.D. dissertation, Virginia Polytechnic Institute and State Univ., Blacksburg, VA, USA, 1994.

[84] C.-H. Chang, C.-A. Cheng, and H.-L. Cheng, "Modeling and design of the LLC resonant converter used as a solar-array simulator," *IEEE Trans. Emerg. Sel. Topics Power Electron.*, vol. 2, no. 4, pp. 833–841, Dec. 2014.

[85] Z. M. Dalala, Z. U. Zahid, O. S. Saadeh, and J.-S. Lai, "Modeling and controller design of a bidirectional resonant converter battery charger," *IEEE Access*, vol. 6, pp. 23338–23350, 2018.

[86] M. F. Menke, Á. R. Seidel, and R. V. Tambara, "LLC LED driver small-signal modeling and digital control design for active ripple compensation," *IEEE Trans. Ind. Electron.*, vol. 66, no. 1, pp. 387–396, Jan. 2019.

[87] N. S. Nise, *Control Systems Engineering*. Hoboken, NJ, USA: Wiley, 2020.

[88] Z. Fang, T. Cai, S. Duan, and C. Chen, "Optimal design methodology for LLC resonant converter in battery charging applications based on time-weighted average efficiency," *IEEE Trans. Power Electron.*, vol. 30, no. 10, pp. 5469–5483, Oct. 2015.

[89] Y. Wei, Q. Luo, Z. Wang, and H. A. Mantooth, "A complete step-by-step optimal design for LLC resonant converter," *IEEE Trans. Power Electron.*, vol. 36, no. 4, pp. 3674–3691, Apr. 2021.

[90] X. Fang et al., "Efficiency-oriented optimal design of the LLC resonant converter based on peak gain placement," *IEEE Trans. Power Electron.*, vol. 28, no. 5, pp. 2285–2296, May 2013.

[91] R. Oruganti and F. C. Lee, "State-plane analysis of parallel resonant converter," in *Proc. IEEE Power Electron. Specialists Conf.*, 1985, pp. 56–73.

[92] M. Bhardwaj and S. Yu, "Bidirectional CLLLC resonant dual active bridge (DAB) reference design for hev/ev onboard charger," Texas Instruments, Dallas, TX, 2020.

[93] Wolfspeed, "22 kW bi-directional high efficiency DC/DC converter," 2020. Accessed: Aug. 11, 2022. [Online]. Available: https://www.wolfspeed.com/crd-22dd12n/

[94] Wolfspeed.com, "6.6 kW high frequency DC-DC converter," 2020. Accessed: Aug. 11, 2022. [Online]. Available: https://www.wolfspeed.com/products/power/reference-designs/crd-06600dd065n/

[95] Texas Innstruments, "Phase shifted full bridge (PSFB) vs. full bridge LLC (FB-LLC) for high power DC/DC conversion," 2018. Accessed: Jan. 20, 2023. [Online]. Available: https://training.ti.com/psfb-vs-fb-llc-part-1?context=1135931-1135928

[96] Battery University, "BU-409: Charging lithium-ion," Sep. 2010. Accessed: Aug. 11, 2022. [Online]. Available: https://batteryuniversity.com/article/bu-409-charging-lithium-ion

[97] Battery University, "BU-201: How does the lead acid battery work?," 2021. Accessed: Mar. 10, 2023. [Online]. Available: https://batteryuniversity.com/article/bu-201-how-does-the-lead-acid-battery-work

[98] F. Musavi, M. Craciun, D. S. Gautam, W. Eberle, and W. G. Dunford, "An LLC resonant DC–DC converter for wide output voltage range battery charging applications," *IEEE Trans. Power Electron.*, vol. 28, no. 12, pp. 5437–5445, Dec., 2013.

[99] R. Beiranvand, B. Rashidian, M. R. Zolghadri, and S. M. H. Alavi, "A design procedure for optimizing the LLC resonant converter as a wide output range voltage source," *IEEE Trans. Power Electron.*, vol. 27, no. 8, pp. 3749–3763, Aug., 2012.

[100] R. Yu, G. K. Y. Ho, B. M. H. Pong, B. W.-K. Ling, and J. Lam, "Computer-aided design and optimization of high-efficiency LLC series resonant converter," *IEEE Trans. Power Electron.*, vol. 27, no. 7, pp. 3243–3256, Jul., 2012.

[101] K. P. Devices, "Considerations for selecting automotive-grade multilayer ceramic capacitors in electric vehicles," Tech. Rep., 2018.

[102] Y. Cui, "Three-phase dual active bridge converter: Design considerations and planar transformer design," Ph.D. dissertation, Department of Electrical and Computer Engineering, McMaster Univ., Hamilton, ON, Canada, 2017.

[103] M. I. Hassan, L. Dorn-Gomba, A. D. Callegaro, M. Narimani, A. Emadi, and M. F. Cruz, "Transformer design optimization for power electronic converters in electric aircraft," in *Proc. IEEE Transp. Electrific. Conf. Expo*, 2020, pp. 402–407.

[104] Z. Ouyang, M. Andersen, and O. Thomsen, "Advances in planar and integrated magnetics," Ph.D. dissertation, Danish Technical Univ., Kongens Lyngby, Denmark, 2011.

[105] A. Kats, G. Ivensky, and S. Ben-Yaakov, "Application of integrated magnetics in resonant converters," in *Proc. APEC 97- Appl. Power Electron. Conf.*, 1997, pp. 925–930.

[106] J. Biela and J. W. Kolar, "Electromagnetic integration of high power resonant circuits comprising high leakage inductance transformers," in *Proc. IEEE 35th Annu. Power Electron. Specialists Conf.*, 2004, pp. 4537–4545.

[107] W. Water and J. Lu, "Improved high-frequency planar transformer for line level control (LLC) resonant converters," *IEEE Magn. Lett.*, vol. 4, 2013, Art. no. 6500204.
[108] R. Shafaei, M. Ordonez, and M. A. Saket, "Three-dimensional frequency-dependent thermal model for planar transformers in LLC resonant converters," *IEEE Trans. Power Electron.*, vol. 34, no. 5, pp. 4641–4655, May 2019.
[109] Y. Zhang, D. Xu, K. Mino, and K. Sasagawa, "1MHz-1 kW LLC resonant converter with integrated magnetics," in *Proc. 22nd Annu. IEEE Appl. Power Electron. Conf. Expo.*, 2007, pp. 955–961.
[110] H. Choi, "Analysis and design of LLC resonant converter with integrated transformer," in *Proc. 22nd Annu. IEEE Appl. Power Electron. Conf. Expo.*, 2007, pp. 1630–1635.
[111] S. Stegen and J. Lu, "Structure comparison of high-frequency planar power integrated magnetic circuits," *IEEE Trans. Magn.*, vol. 47, no. 10, pp. 4425–4428, Oct. 2011.
[112] W. Water, "Modelling and design of advanced high frequency transformers," Ph.D. dissertation, Griffith School of Environment, Griffith Univ., Brisbane, QLD, Australia, 2013.
[113] R. Chen, J. T. Strydom, and J. D. van Wyk, "Design of planar integrated passive module for zero-voltage-switched asymmetrical half-bridge PWM converter," *IEEE Trans. Ind. Appl.*, vol. 39, no. 6, pp. 1648–1655, Nov./Dec. 2003.
[114] J. Biela and J. W. Kolar, "Using transformer parasitics for resonant converters–A review of the calculation of the stray capacitance of transformers," in *Proc. 14th IAS Annu. Meeting Conf. Rec. Ind. Appl. Conf.*, 2005, pp. 1868–1875.
[115] X. Zhao, C.-W. Chen, J.-S. Lai, and O. Yu, "Circuit design considerations for reducing parasitic effects on GaN-based 1-MHz high-power-density high-step-up/down isolated resonant converters," *IEEE J. Emerg. Sel. Topics Power Electron.*, vol. 7, no. 2, pp. 695–705, Jun. 2019.
[116] M. A. Saket, N. Shafiei, and M. Ordonez, "LLC converters with planar transformers: Issues and mitigation," *IEEE Trans. Power Electron.*, vol. 32, no. 6, pp. 4524–4542, Jun. 2017.
[117] M. A. Saket, M. Ordonez, M. Craciun, and C. Botting, "Improving planar transformers for LLC resonant converters: Paired layers interleaving," *IEEE Trans. Power Electron.*, vol. 34, no. 12, pp. 11813–11832, Dec. 2019.
[118] R. Beiranvand, B. Rashidian, M. R. Zolghadri, and S. M. H. Alavi, "Using LLC resonant converter for designing wide-range voltage source," *IEEE Trans. Ind. Electron.*, vol. 58, no. 5, pp. 1746–1756, May 2011.
[119] R. Beiranvand, B. Rashidian, M. R. Zolghadri, and S. M. H. Alavi, "Optimizing the normalized dead-time and maximum switching frequency of a wide-adjustable-range LLC resonant converter," *IEEE Trans. Power Electron.*, vol. 26, no. 2, pp. 462–472, Feb. 2011.
[120] Y. Wei, Q. Luo, Z. Wang, and H. A. Mantooth, "Simple and effective adaptive deadtime strategies for LLC resonant converter: Analysis, design, and implementation," *IEEE Trans. Emerg. Sel. Topics Power Electron.*, vol. 10, no. 2, pp. 1548–1562, Apr. 2022.
[121] R. Pradhan, N. Keshmiri, and A. Emadi, "On-board chargers for high-voltage electric vehicle powertrains: Future trends and challenges," *IEEE Open J. Power Electron.*, vol. 4, pp. 189–207, 2023.
[122] Infineon.com, "Power MOSFET," 2023. Accessed: Sep. 25, 2023. [Online]. Available: https://www.infineon.com/cms/en/product/power/mosfet/
[123] G. N. Love and A. R. Wood, "Harmonic state space model of power electronics," in *Proc. IEEE 13th Int. Conf. Harmon. Qual. Power*, 2008, pp. 1–6.
[124] J. Kwon, X. Wang, F. Blaabjerg, C. L. Bak, V.-S. Sularea, and C. Busca, "Harmonic interaction analysis in a grid-connected converter using harmonic state-space (HSS) modeling," *IEEE Trans. Power Electron.*, vol. 32, no. 9, pp. 6823–6835, Sep. 2017.
[125] J. W. Bandler, R. M. Biernacki, S. H. Chen, P. A. Grobelny, and R. H. Hemmers, "Space mapping technique for electromagnetic optimization," *IEEE Trans. Microw. Theory Techn.*, vol. 42, no. 12, pp. 2536–2544, Dec. 1994.
[126] G. A. Mudiyanselage, N. Keshmiri, M. Bakr, and A. Emadi, "Modeling and control optimization of a three-port resonant converter using space mapping optimization," in *Proc. IEEE Transp. Electrific. Conf. Expo*, 2023, pp. 1–6.
[127] A. Frances, R. Asensi, and J. Uceda, "Blackbox polytopic model with dynamic weighting functions for DC-DC converters," *IEEE Access*, vol. 7, pp. 160263–160273, 2019.

GUVANTHI ABEYSINGHE MUDIYANSELAGE (Student Member, IEEE) received the B.Sc. degree in electrical engineering from the University of Moratuwa, Moratuwa, Sri Lanka, in 2016, and the master's degree in electrical engineering and the Ph.D. degree from McMaster University, Hamilton, ON, Canada. From 2016 to 2019, she was an Electrical Engineer with Ceylex Engineering Pvt. Ltd., Colombo, Sri Lanka, working on high voltage grid substation designing, testing and commissioning. She started her master's degree in electrical engineering in 2020 and later transferred to Ph.D. degree in 2021 with McMaster University. Her research interests include design and control of two-port and three-port DC-DC converters for electrified transportation applications.

NILOUFAR KESHMIRI (Student Member, IEEE) received the B.Eng. and Management degrees in electrical engineering and management from McMaster University, Hamilton, ON, Canada, in 2018, and the Ph.D. degree in electrical and computer engineering from McMaster University, in 2023, while working with the McMaster Automotive Resource Centre. She has worked on several projects focusing on the design of high performance and efficient power electronic converters for aerospace and electric vehicle applications. She is currently the Project Manager of the McMaster EcoCAR Electric Vehicle Challenge. Her research interests include the design, control, and optimization of power electronics converters in electrified transportation applications. She specializes in high efficiency converter systems using Gallium Nitride (GaN) wide bandgap semiconductor technology.

ALI EMADI (Fellow, IEEE) received the B.S. and M.S. degrees (with highest distinction) in electrical engineering from the Sharif University of Technology, Tehran, Iran, in 1995 and 1997, respectively, and the Ph.D. degree in electrical engineering from Texas A&M University, College Station, TX, USA, in 2000. He is the Canada Excellence Research Chair Laureate with McMaster University, Hamilton, ON, Canada. He is also the NSERC/FCA Industrial Research Chair of Electrified Powertrains and Tier I Canada Research Chair in Transportation Electrification and Smart Mobility. Before joining McMaster University, he was the Harris Perlstein Endowed Chair Professor of Engineering and the Director of the Electric Power and Power Electronics Center and Grainger Laboratories, Illinois Institute of Technology in Chicago, Chicago, IL, USA, where he established research and teaching facilities as well as courses in power electronics, motor drives, and vehicular power systems. He was the Founder, Chairman, and President of Hybrid Electric Vehicle Technologies, Inc. (HEVT)—a university spin-off company of Illinois Tech. He is currently the President and Chief Executive Officer of Enedym Inc. and Menlolab Inc.—two McMaster University spin-off companies. He is the Principal author or co-author of more than 500 journal and conference papers as well as several books, including *Vehicular Electric Power Systems* in 2003, *Energy Efficient Electric Motors* in 2004, *Uninterruptible Power Supplies and Active Filters* in 2004, *Modern Electric, Hybrid Electric, and Fuel Cell Vehicles* (2nd ed) in 2009, and *Integrated Power Electronic Converters and Digital Control* in 2009. He is also the Editor of the *Handbook of Automotive Power Electronics and Motor Drives* in 2005, and *Advanced Electric Drive Vehicles* in 2014. He is the co-editor of the *Switched Reluctance Motor Drives* in 2018. Dr. Emadi was the Inaugural General Chair of the 2012 IEEE Transportation Electrification Conference and Expo (ITEC) and has chaired several IEEE and SAE conferences in the areas of vehicle power and propulsion. He was the founding Editor-in-Chief of IEEE TRANSACTIONS ON TRANSPORTATION ELECTRIFICATION from 2014 to 2020.